One-step induction of human GABAergic neurons promotes presynaptic development & synapse maturation

Torben W. van Voorst[1,+], Maaike A. van Boven [1,+], Kevin I. Marinus[2,+], Jennifer M. Colón-Mercado[3], Jule Schretzmeir[1], Carolin Haag[1,4], Ruud F. Toonen[1,4], Frank Koopmans[2], Michael E. Ward[3], August B. Smit[2], Ronald E. van Kesteren[2], Matthijs Verhage[1,4,5], L. Niels Cornelisse[1,5,#]

[1]Department of Functional Genomics, Center for Neurogenomics and Cognitive Research (CNCR), VU University Amsterdam, de Boelelaan 1100, 1081 HZ Amsterdam, The Netherlands.

[2]Department of Molecular and Cellular Neurobiology, Center for Neurogenomics and Cognitive Research (CNCR), VU University Amsterdam, de Boelelaan 1100, 1081 HZ Amsterdam, The Netherlands.

[3]National Institute of Neurological Disorders and Stroke, National Institutes of Health, 9000 Rockville Pike, Bethesda, MD, USA

[4]Neurospector, de Boelelaan 1100, 1081 HZ Amsterdam, The Netherlands.

[5]Department of Human Genetics, Amsterdam UMC – location VU University Amsterdam, de Boelelaan 1100, 1081 HV Amsterdam, The Netherlands.

[+] Authors contributed equally

[#] Correspondence: l.n.cornelisse@vu.nl

Abstract (169 words)

Human induced pluripotent stem cells (iPSCs) present a powerful approach to study human brain physiology and disease, yet robust, pure GABAergic induction has remained difficult. Here we present improved, single-step, transposon-based GABAergic induction with Ascl1/Dlx2, which yields, unlike lentiviral approaches, exclusively GABAergic neurons and was validated across three independent iPSC lines. Co-seeding with Ngn2-induced excitatory neurons created stable networks of predefined excitation/inhibition ratios, with corresponding synapse ratios. Proteomic and electrophysiological characterization at different developmental time points showed that the single-step induced GABAergic neurons gain a proteomic profile that maps to different cortical interneuron subtypes and display typical GABAergic synaptic properties, producing large, synchronous and picrotoxin-sensitive currents. During early development, synaptic strength increased threefold, which was accompanied by an increase in expression of proteins exclusively enriched for presynaptic

SYNGO terms. Synaptic strength continued to increase during late development but with only minor proteomic changes. Taken together, transposon-based GABAergic induction yields exclusively mature GABAergic neurons suitable for studying genes involved in synaptic maturation and to build excitation/inhibition networks for disease modelling.

Keywords (max 10)

Induced pluripotent stem cells, induced GABAergic neurons, Transposon, Synaptic maturation, Ascl1, Dlx2, Autaptic neurons, Proteomics, Patch-clamp, Excitation/inhibition

Introduction

Human induced pluripotent stem cell (iPSC)-derived models provide a promising platform for studying human brain physiology and pathology. iPSCs can be generated from patient-derived tissue or blood to better reflect the human genetics and (patho)physiology compared to commonly employed rodent models.[1-3] GABAergic dysfunction and excitation/inhibition (E/I) disbalance have been implicated in many neurodevelopmental and neurodegenerative disorders.[4-9] In recent years, various strategies have been developed for generating iPSC-derived GABAergic neurons, but robust, pure GABAergic induction remains challenging. Directed differentiation, which employs signalling molecules to mimic neurodevelopment.[10-12], yields both glutamatergic and GABAergic neurons, but these type of inductions often generate inconsistent E/I ratios, tend to yield heterogeneous and immature neuronal populations and are costly and time-consuming.[13] Rapid differentiation approaches rely on overexpression of key transcription factors, such as Ascl1 and Dlx2 for GABAergic differentiation.[14,15] and often rely on lentiviral delivery of transgenes. However, such approaches have several limitations: (1) they require multiple vectors when delivering multiple transgenes due to the size cap of ~8 kb, (2) they pose a risk of disrupting host genes[16], and (3) they are susceptible to epigenetic silencing during prolonged iPSC culturing [17-19] To overcome these challenges, TALEN- and CRISPR-based gene editing.[20] have been used to target the transgenes to the *AAVS1* safe harbor locus[21,22] While this ensures stable transgene expression, allows for delivery of multiple genes in a single construct, and minimizes off-target effects, it is time and resource-consuming due to the need for clonal expansion and extensive validation of every iPSC line used in a study.[23]

The PiggyBac transposon system has emerged as a gene-delivery tool that overcomes most of these limitations. Unlike lentiviral systems, transposons enable stable genomic integration of large genetic constructs up to 200 kb.[24] through a "cut-and-paste"

mechanism[25], which enables delivery of multiple transgenes in a single construct. Additionally, transposon-delivered transgenes are less prone to silencing than lentivirally delivered transgenes[26] and the increased packing capacity permits the inclusion of epigenetic regulators to further diminish silencing. Compared to safe harbor insertion of transgenes, the delivery of a transposon cassette is a simpler, single-step process applicable to multiple iPSC lines in parallel and allows the use of a polyclonal population for most use cases, eliminating the need for thorough validation, thereby accelerating experimental timelines.

Here, we characterize PiggyBac transposon-based overexpression of *Ascl1* and *Dlx*2 (PB-AD) for GABAergic neuronal induction and benchmark this against established GABAergic induction methods. PB-AD-based induction results in exclusively GABAergic differentiation across different genetic backgrounds, unlike lentiviral approaches which induce both GABAergic and glutamatergic differentiation. We demonstrate that PB-AD neurons integrate into synaptically connected E/I networks when co-cultured with excitatory NGN2 neurons with synaptic projections proportional to cellular ratios. Using proteomics, patch-clamp electrophysiology, and immunocytochemistry we show that PB-AD induction yields neurons with reliable, plastic synapses that synchronously release GABA and strengthen during prolonged culture, with pronounced presynaptic proteomic changes. We propose that this improved GABAergic induction protocol, which reliably generates pure GABAergic neurons, enables the study of human GABAergic functioning in pure GABAergic networks, in single-neuron (autaptic) cultures, and stable E/I-networks.

Results

GABAergic differentiation of human iPSCs using PiggyBac based delivery of Ascl1 and Dlx2

Overexpression of the transcription factors Ascl1 and Dlx2 drives GABAergic lineage specification of induced pluripotent stem cells (iPSCs)[15] Previous approaches employed separate lentivectors to express both genes in an inducible manner. We aimed to develop a simplified GABAergic differentiation protocol using a single PiggyBac transposon construct containing both transcription factors (RRID: Addgene_182307,Figure 1A). This vector contains (1) a doxycycline (dox)-inducible expression cassette for *Ascl1* and *Dlx2* from a bidirectional promoter, avoiding variation in expression levels resulting from position effects in multi-cistronic vectors; (2) reverse tetracycline-controlled transactivator (rtTA), required for dox-inducible expression; (3) the puromycin resistance gene (pac), allowing for antibiotic selection, as well as (4) mTagBFP2[27], giving transfected cells a fluorescent marker; and (5)

Ubiquitous Chromatin Opening Elements (UCOE)[28] and 5'HS chicken β-globin (cHS4) insulator elements.[29] Firstly, we tested whether our newly designed construct could induce GABAergic differentiation (Figure 1B). To this end, we co-transfected this PiggyBac vector with a transposase vector into BIONi010-C iPSCs.[30] After puromycin-selection, all cells expressed mTagBFP2 (Figure 1C), confirming successful transgene integration. Upon dox-induction, cells first clustered together (Figure 1D) and after releasing and reseeding at 3 days post-induction (DPI), cells developed a neuronal morphology, which became more distinct within one week (Figure 1E). At 10 weeks post-induction (WPI), neurons displayed MAP2+ dendrites and $VGAT^+$ puncta, indicative of GABAergic synapses, whereas glutamatergic $VGLUT1/2^+$ puncta were absent (Figure 1F,G).

GABAergic synaptic transmission in PiggyBac Ascl1/Dlx2 neurons

To confirm the GABAergic identity of PiggyBac-induced neurons we performed voltage-clamp recordings in autaptic cultures.[31] between 6 and 10 WPI (Figure 1H). Rapid depolarization to +30 mV induced action potential evoked postsynaptic currents (ePSCs), which displayed slow decay times (τ) characteristic of GABAergic currents[32], as determined by mono-exponential fits (geometric mean (GM) = 104.2 ms, geometric SD factor (GM_{SDf}) = 1.42; Figure 1I,J). Furthermore, virtually all synaptic signalling was abolished after applying the GABA receptor antagonist picrotoxin (PTX), confirming GABAergic synaptic identity (Figure 1I,K).

PiggyBac Ascl1/Dlx2 yields a pure GABAergic neuron population in contrast to lentiviral methods

To benchmark the PiggyBac approach, we compared it with two established lentiviral methods for GABAergic induction[14,15], and an NGN2-based protocol for glutamatergic induction[22,33] (Figure 1L). Autaptic neurons were generated using all four protocols and ePSC decay time constants were quantified using mono-exponential fits. As expected, NGN2-derived neurons exhibited fast ePSCs decay kinetics typical of glutamatergic transmission (GM = 2.43 ms, GM_{SDf} = 1.39, Figure 1M,N), confirmed pharmacologically and by the presence of $VGLUT1/2^+$ puncta (Figure S1). Surprisingly, decay time constants from neurons generated with the lentiviral GABAergic protocols showed a bimodal distribution which could be fitted with a sum of two gaussians. More than half of the cells in these cultures exhibited ePSC kinetics comparable to those in the NGN2 cultures (Lenti AF: GM = 2.82 ms, GM_{SDf} = 0.58, 72.8% of the fit; Lenti AD: GM = 4.62 ms, GM_{SDf} = 0.42, 55.3% of the fit). The remaining cells had more than tenfold larger time constants typical for slow GABAergic ePSCs (Lenti AF: GM = 86.3 ms, GM_{SDf} = 1.56 for 27,2% of the fit; Lenti AD: GM = 60.5 ms, GM_{SDf} = 1.26 for 44.7% of the fit). In contrast, the PB-AD method produced a unimodal population with slowly decaying ePSCs (GM = 78.9 ms, GM_{SDf} = 1.35). Since NGN2 and PB-AD neurons produced decay time

constants with unimodal fits, these values were used to determine cut-off thresholds for synaptic identity (glutamatergic: $\tau \leqslant 6$ ms; GABAergic: $\tau \geqslant 30$ ms; mixed: $6 < \tau < 30$ ms). This revealed that 68% of PB-AD neurons exhibited GABAergic currents, while the remaining 32% were synaptically silent (Figure 1O). In contrast, the lentiviral approaches generated a substantial population of glutamatergic (Lenti AF: 43%, Lenti AD: 39%) and mixed (Lenti AF: 9% Lenti AD: 15%) identities. The consistent generation of functional GABAergic neurons and the absence of glutamatergic neurotransmission underscore the reliability of the PB-AD protocol compared to previously described methods.

PiggyBac Ascl1/Dlx2 protocol induces GABAergic neurons across genetic backgrounds

To test for generalizability, we applied the PB-AD protocol to generate neurons from two additional iPSC lines, KOLF2.1J[34] and GM23973[35], and characterized their functional properties at 7 and 6 WPI, respectively. In both lines the PB-AD approach produced neurons with GABAergic synaptic projections and slow-decaying synaptic transmission, indicative of GABAergic specification (Figure S2), as was found for the BIONi010-C line. These findings demonstrate the protocol's applicability across genetic backgrounds.

PiggyBac Ascl1/Dlx2 neurons integrate into controlled excitatory/inhibitory networks

To test whether PB-AD neurons integrate into E/I networks alongside glutamatergic neurons, we co-cultured 3 DPI PB-AD neurons with 3 DPI glutamatergic NGN2 neurons in networks containing 100%, 30% (as found in the human cortex[36-38]) and 0% inhibitory neurons (Figure 2A-C). Immunocytochemistry at 10 WPI (Figure 2B,C) revealed comparable neuronal cell densities across all conditions, as measured by NeuN staining, indicating similar viability of PB-AD and NGN2 neurons. (Figure 2D). Total dendrite length per field of view increased as the proportion of PB-AD neurons decreased, consistent with the distinct morphological characteristics of GABAergic neurons[39] (Figure 2E). Pure PB-AD networks contained $VGAT^+$ (GABAergic) synaptic puncta, and NGN2 networks contained $VGLUT1/2^+$ (glutamatergic) synaptic puncta, with in both cases virtually no puncta of the other type present (Figure 2F,G). In contrast, the mixed (30% PB-AD) networks contained both GABAergic and glutamatergic puncta on the same dendrite proportional to cellular ratios, demonstrating that PB-AD neurons are viable components for assembling E/I networks when mixed with NGN2 neurons.

PiggyBac Ascl1/Dlx2 neurons acquire a GABAergic molecular identity over time

Next, we assessed differentiation of PB-AD and NGN2 neurons over time using mass spectrometry-based proteomics. PB-AD co-cultures with rat astrocytes were compared to NGN2 co-cultures at 4, 6, 8, and 10 WPI (Figure 3A). We detected 99,154 human peptide

170 precursors mapping to 7,775 unique proteins across 60 samples that passed quality control.
171 Variability within groups was low-to-moderate with coefficients of variation between 14.6%
172 and 32.2%, reflecting consistent detection across replicates (Figure S3A-B). To remove rat
173 astrocytic signal, subsequent analyses focused on neuronally enriched proteins (1690
174 proteins), which show >70% neuron-specific expression according to single-cell
175 transcriptomics data of the human cortex (Jostad). Principal component analysis (PCA) on the
176 neuronally-enriched protein abundances (Figure 3B, S3C) revealed clear separation between
177 PB-AD and NGN2 cultures along the first two components (PC1: 71.5% and PC2: 6.1%), as
178 well as the separation of different time points within each culture. More specifically, time
179 points from both PB-AD and NGN2 cultures showed clear separation between 4, 6, and 8 WPI,
180 while cultures at 8 and 10 WPI clustered more closely together, suggesting that proteomic
181 maturation plateaus after 8 weeks.

182 To assess lineage specification of PB-AD and NGN2 inductions, we annotated cell
183 types based on differentially expressed proteins using cell type specificity scores (CTSS),
184 computed using single-cell RNA expression data from human cortex[40] (Figure S4A). Across
185 all timepoints, canonical GABAergic proteins, including SLC32A1 (VGAT), GAD1, GAD2, were
186 enriched in PB-AD cultures. In addition, other predicted GABAergic proteins, such as CRHBP,
187 FBN2, CRH, and RELN, were enriched in PB-AD neurons. In contrast, only a few predicted
188 glutamatergic proteins (e.g., BDNF, PCP4, CPZ, and ADAMTSL1) were moderately enriched in
189 PB-AD cultures. The glutamatergic marker SLC17A6 (VGLUT2) was enriched in NGN2 cultures,
190 while SLC17A7 (VGLUT1) was not detected (Figure 3C-F). Surprisingly, NGN2 neurons also
191 showed strong enrichment of several proteins typically associated with GABAergic neurons
192 at all timepoints, including SCGN, CALB2, and PVALB. Immunocytochemistry confirmed PVALB
193 expression in the majority of NGN2 neurons (Figure S4B).

194 To quantitatively assess cell type specification, we performed expression-weighted
195 cell type enrichment (EWCE) analysis[41] on the top 5% upregulated neuronal proteins for each
196 induction for each timepoint. At all timepoints, PB-AD-specific neuronal proteins showed
197 exclusive and significant enrichment for GABAergic neurons, with enrichment levels
198 increasing until 8 WPI (Figure 3G). GABAergic subclass analysis revealed strongest
199 enrichment for VIP^+ interneurons from 6-10 WPI (Figure S4C). In contrast, NGN2-specific
200 proteins showed significant enrichment for glutamatergic neurons only at 6 and 10 WPI,
201 while also displaying unexpected GABAergic enrichment, reaching significance at 4 and 10
202 WPI (Figure 3H). Subclass enrichment analysis revealed that this unexpected GABAergic
203 enrichment was most likely accounted for by $PVALB^+$ and VIP^+ interneuron-like profiles (S4C,

204 S4D). Taken together, PB-AD neurons acquire a stable GABAergic identity over time,
205 characterized by consistent expression of canonical and subtype-specific GABAergic proteins.
206 By contrast, NGN2-induced neurons exhibit a mixed molecular identity, with evidence for
207 partial GABAergic specification in addition to expected glutamatergic features.

208 *Gradual morphological development of PiggyBac Ascl1/Dlx2 neurons*

209 To examine morphological maturation of PB-AD neurons, we performed immunostaining for
210 MAP2, VGAT and VGLUT1/2 in autaptic cultures (Figure S5A,B). Similar to networks, PB-AD
211 neurons produced only $VGAT^+$ puncta at all timepoints (Figure S5A,B, Figure 4A-C). A
212 progressive increase in dendrite length was observed during maturation (Figure 4B),
213 accompanied by an increase in the total number of $VGAT^+$ puncta per neuron and puncta
214 densities per dendritic length (Figure 4C,D). Additionally, the intensities of VGAT puncta
215 increased over time (Figure 4E), suggesting increased synaptic vesicles per synaptic terminal.
216 Sholl analysis revealed a rise in the number of arborizations during maturation (Figure
217 S5C,D,I). Interestingly, growth of dendritic length and complexity plateaued by 6 WPI,
218 whereas synaptic projections continued to develop until 8 and 10 WPI. Together, these results
219 demonstrate that PB-AD neurons develop complex neuronal morphologies accompanied by
220 an increase in presynaptic GABAergic terminals during maturation.

221 *Synaptic strengthening during maturation of PiggyBac Ascl1/Dlx2 neurons*

222 Next, we assessed functional maturation in autaptic neurons with voltage-clamp
223 electrophysiology. Firstly, action-potential independent spontaneous release was recorded.
224 Both miniature postsynaptic current (mPSC) frequency and amplitude increased during
225 maturation (Figure 4F-H). Next, neurons were depolarized to induce ePSCs. Across all time
226 points, 70-80% of neurons were synaptically active, producing a charge of at least 1.5 pC
227 within 70 ms after stimulation (Figure 4I). In active cells, both the amplitude and charge of
228 ePSCs increased progressively between 4 and 10 WPI (Figure 4J-L), with the most pronounced
229 change occurring from 8 to 10 WPI. Decay constants remained consistently above 30 ms –
230 characteristic of GABAergic currents (Figure 4M). Interestingly, decay kinetics subtly slowed
231 after 4 WPI, suggesting potential changes in postsynaptic receptor subunits.[42,43]

232 To evaluate the impact of maturation on short-term synaptic plasticity, we applied
233 paired-pulse stimulation at 50 ms, 200 ms, and 1000 ms intervals (Figure S5E-H). This
234 revealed modest synaptic depression which was stable throughout maturation. Only at a
235 1000 ms interval, synaptic depression increased as neurons matured. Importantly, maturation
236 increased the size of the readily releasable pool (RRP), as determined by back-extrapolation
237 of the charge evoked by 20 Hz stimulus trains, with the biggest change occurring from 8 to

238 10 WPI (Figure S5I-K). Taken together, these findings demonstrate that PB-AD GABAergic
239 neurons develop functional, plastic synapses that strengthen during maturation.

240 *Functional maturation correlates with upregulation of proteins in presynaptic gene sets*
241 To investigate the molecular basis of synaptic maturation, we looked at the differential
242 expression of SYNGO-annotated synaptic proteins[44] between different timepoints of
243 development (4 to 6 WPI, 6 to 8 WPI, and 8 to 10 WPI) (Figure 5A). Of all 1605 SYNGO-
244 annotated synaptic genes, 929 unique proteins were detected in PB-AD cultures, of which
245 478 (51%) were differentially expressed in at least one time contrast (Figure 5B, D-F). In
246 NGN2 neurons, 967 unique SYNGO-annotated proteins were identified of which 644 (67%)
247 were differentially expressed in at least one time contrast (Figure 5C, Figure S6A-C). In both
248 cultures, SYNGO-annotated proteins were abundantly regulated between 4 and 8 WPI, while
249 only few proteins showed altered expression between 8 and 10 WPI (Figures 5B-F,
250 Supplementary table 1). This indicates that proteomic synaptic maturation plateaus after 8
251 WPI, consistent with what was observed for neuronal-enriched protein expression.
252 To examine specifically how pre- and postsynapses develop over time, we used GOAT[45]
253 to determine which SYNGO gene sets were enriched for developmentally regulated proteins,
254 where the contribution of each protein was weighted by its $\log_2$(fold change).[45] Strongest
255 enrichment was observed between 4-6 WPI and 6-8 WPI, which occurred exclusively in
256 presynaptic gene sets, including *synaptic vesicle* (*SV*), *presynaptic active zone (AZ)*, and
257 *presynaptic membrane* (Figure 5G-L). Between 8-10 WPI only *SV membrane* proteins and its
258 mother term *presynaptic* proteins were enriched. In contrast, no postsynaptic gene sets were
259 significantly enriched in PB-AD cultures, across all time contrasts. To exclude that these
260 results were biased by a few proteins with large effect sizes, additional SYNGO gene set
261 overrepresentation analysis was performed based on the number of upregulated proteins
262 per gene set. This confirmed the exclusive enrichment of presynaptic terms in PB-AD cultures
263 (Figure S6J–L). Upregulated proteins in NGN2 cultures over time similarly showed a
264 preferential enrichment of presynaptic gene sets using GOAT and SYNGO overrepresentation
265 analyses, with no enrichment for postsynaptic gene sets between 6-10 WPI. Thus, synaptic
266 strengthening correlates with changes specifically in presynaptic protein levels, while
267 postsynaptic protein levels remain relatively stable over time.
268 In order to test whether our findings on asymmetrical pre- and postsynaptic
269 maturation translate to a more physiological model, we assessed postsynaptic responses to
270 externally applied GABA in E/I networks, as excitation might alter maturation profiles.[46]
271 (Figure 5M). Furthermore, we used gramicidin-perforated patch to allow measurement of

272 postsynaptic responses without influencing the reversal potential for the GABA-receptor[47]
273 GABA puffs were applied at varying holding voltages (Figure 5N). The slope of the I/V curve
274 voltages was unaltered by maturation ($p = 0.305$), indicating that the GABAergic postsynaptic
275 response does not change during maturation under these conditions. Thus, increased
276 synaptic strength during synaptic maturation correlates with presynaptic proteomic changes,
277 but not with postsynaptic development also in E/I-networks.

278 *PiggyBac Ascl1/Dlx2 specific synaptic proteins map to cortical interneuron subtypes*
279 Finally, we investigated whether changes in PB-AD and NGN2 SYNGO-annotated proteomes
280 between 4 and 10 WPI are associated with cortical GABAergic and glutamatergic cell types.[40]
281 (Figure 6A). PB-AD cultures showed upregulation of predicted GABAergic and medial
282 ganglionic eminence (MGE) and caudal ganglionic eminence (CGE)-specific proteins (Figure
283 6B). NGN2 cultures showed upregulation of predicted glutamatergic proteins (Figure 6C). Of
284 note, PB-AD and NGN2 cultures showed upregulation of both GABAergic and glutamatergic
285 receptor subunits (Figure S7A,B), although only input of one of the neurotransmitters was
286 present per culture. Canonical subtype markers for both MGE- and CGE-derived subtypes
287 were also detected in PB-AD neurons (S7C,D).
288 To analyze lineage-specific synaptic development in more detail, we next contrasted
289 the developing (WPI 4 to WPI 10) PB-AD and NGN2 SYNGO-annotated proteomes with each
290 other to find proteins that were specifically regulated in each induction. To this end, for each
291 protein we calculated the difference between PB-AD and NGN2 in differential expression
292 between 4-10 WPI (i.e., $\log_2 (FC)_{AD} - \log_2 (FC)_{NGN2}$), and selected the 5th and 95th percentile to
293 define induction-specific synaptic proteins (Figure 6A). We then assessed whether these
294 proteins were enriched in either cortical glutamatergic or cortical GABAergic reference
295 expression profiles[40] Overall, this produced lineage-specific enrichments in most gene sets.
296 PB-AD specific synaptic proteins showed the highest GABAergic enrichment in the gene sets
297 *dense core vesicle* (*DCV*), *SV*, *synaptic signalling*, *metabolism* and *presynaptic process* (Figure 6D-
298 E). Conversely, NGN2-specific synaptic proteins that belonged to *synaptic signalling, SV,*
299 *organization* and *specialization* showed the highest glutamatergic enrichment (Figure 6F-G).
300 As synaptic gene expression profiles have been shown to reflect neuronal subtypes[48],
301 we queried whether synaptic proteins that specifically increase in PB-AD or NGN2 cultures
302 show enrichment for neuronal (sub)types. In EWCE analysis, the PB-AD-specific synaptic
303 proteins were enriched in GABAergic neurons (Figure 6H), specifically VIP$^+$, SST$^+$, PAX6$^+$ and
304 LAMP5$^+$ interneurons, but not PVALB$^+$ neurons (Figure 6I). NGN2-specific synaptic proteins
305 were enriched in glutamatergic subtypes (IT, L4 IT, L5 ET, L6 CT, and L6b) but also in

306 GABAergic subtypes (Figure 6J), particularly VIP$^+$ interneurons (Figure 6K). Together, these
307 data indicate that PB-AD-based induction leads to GABAergic synaptic specialization with
308 molecular profiles resembling CGE- and MGE-derived interneurons, whereas NGN2 induction
309 leads to induction of neurons that also contain typical GABAergic proteins.
310

311 **Discussion**

312 *Summary*

313 In this work, we present a single-step, transposon-based GABAergic differentiation method,
314 which uses a single vector to overexpress Ascl1/Dlx2, and we provide a detailed
315 characterization of these GABAergic neurons at different developmental timepoints using
316 mass spectrometry proteomics, immunocytochemistry, and patch-clamp electrophysiology.
317 This method is applicable across different genetic backgrounds and produces exclusively
318 GABAergic neurons with a proteomic profile that maps to different cortical interneuron
319 subtypes, particularly VIP$^+$ neurons. Synapses display GABAergic properties such as
320 picrotoxin-sensitive, slowly decaying, evoked postsynaptic currents and short-term
321 depression, similar to primary GABAergic neurons.[49-53] During development, synapses
322 gradually increase in synaptic strength, which at earlier timepoints correlates with increased
323 expression of presynaptic proteins associated with active zone, synaptic vesicle, and
324 presynaptic membrane gene sets. In contrast, little functional and proteomic changes occur
325 in the postsynapse. Late in development, synaptic strength continues to increase, with only
326 minor proteomic changes. PB-AD neurons can be combined with NGN2 neurons to form
327 networks of predefined E/I ratios with corresponding synapse ratios. Taken together,
328 transposon-based GABAergic induction yields GABAergic neurons with improved synaptic
329 properties that can be used to build balanced excitation/inhibition networks, for instance to
330 model diseases in which E/I disbalance has been proposed as a disease mechanism.

331 *PiggyBac Ascl1/Dlx2 neuronal induction produces exclusively GABAergic neurons*

332 By employing autaptic neurons we were able to detect synaptic output on a single neuron
333 scale, which allowed us to accurately quantify lineage specification and demonstrate how
334 GABAergic transposon-based induction compares to lentiviral strategies. Previous studies
335 using a lentiviral approach also detected non-GABAergic currents[54] and reported expression
336 of glutamatergic genes[55,56], while others focused on measurements in E/I-networks[14,15] or
337 recorded under conditions that blocked glutamatergic transmission[57,58], making it difficult to
338 compare with our results. As Ascl1 expression, by itself, induces glutamatergic
339 differentiation[59,60], the balance of Ascl1 and Dlx2 expression is likely important in steering

differentiation towards a GABAergic fate. The design of our transposon-based induction incorporates multiple features to facilitate this and thereby avoids unwanted glutamatergic specification. Firstly, both factors are present in one cassette and transcribed from a bidirectional promotor. Secondly, a shared integration site could prevent position effects.[61] Lastly, insulator elements may reduce gene silencing, which is observed for lentiviral cargo[17-19,62-65], and less so for transposon delivered transgenes.[26]

Proteomic profiles of PiggyBac Ascl1/Dlx2 neurons map to cortical interneuron subtypes

Cell type enrichment analysis revealed that neuronal proteins that are higher expressed in PB-AD cultures are significantly enriched for GABAergic neurons at all timepoints, with specific enrichment for VIP$^+$ interneurons from 6 WPI onwards. Zooming in on synaptic proteins that are upregulated specifically in PB-AD cultures between 4-10 WPI, we showed significant enrichment for all GABAergic interneuron subtypes except PVALB$^+$, suggesting specification towards both MGE- and CGE-derived neurons. Assessment of the neuronal lineages produced by PB-AD induction would require single-cell sequencing approaches. A previous single-cell RNA-sequencing study of lenti AD neurons predominantly found SST$^+$ neurons at 4 WPI, but later time points were not investigated.[66] Perhaps CGE markers only appear further along the maturation process, or transcriptomics do not accurately reflect the molecular identity of these neurons.[67-69] To further restrict and direct subtype specification during PB-AD induction, additional patterning with small molecules, which was recently developed for safe harbor-AD induction, could potentially be employed.[70]

Ngn2-induction produced cultures with a mixed glutamatergic and GABAergic molecular identity, including canonical GABAergic markers such as SCGN, PVALB, CALB2. Although these markers are sometimes found in certain glutamatergic neurons in the brain[71-76], it is more likely that their expression is a result of nonspecific differentiation. Nevertheless, virtually no VGAT puncta were identified and only glutamatergic ePSCs were recorded, consistent with previous reports.[21,77-82]

Enhanced expression of presynaptic proteins during synaptic maturation

Our multilevel analysis of GABAergic cultures at different time points between 4 and 10 WPI, combining patch-clamp electrophysiology, immunocytochemistry, and mass spec proteomics, revealed the following insights about synapse maturation. Firstly, synaptic strength increased approximately 3-fold during this period. A comparable increase in mPSC frequency and RRP suggests that this is due to an increase in the strength and/or number of presynaptic projections, which is further supported by VGAT immunocytochemistry. This developmental

373 trajectory is similar to what has been described for directed-differentiation and safe harbor
374 AD GABAergic autaptic neurons.[33,79]
375 Secondly, we observed a stark difference between pre- and postsynaptic molecular
376 differentiation. Strong upregulation of *AZ*-, *SV*- and *presynaptic membrane* proteins occurred,
377 while expression changes in proteins in postsynaptic gene sets were minimal. Asymmetric
378 proteomic development of the pre- and postsynapse was also observed in NGN2 neurons
379 and has been described for iPSC-derived neurons obtained through directed
380 differentiation.[83,84] In PB-AD neurons, current responses to GABA puffs remained constant
381 over time, indicating that functional postsynapses already exist at 4 WPI and the expression
382 of GABA receptors remains unaltered at subsequent weeks. This fits with the notion that
383 expression of postsynaptic neurotransmitter receptors precedes presynaptic innervation.[85-89]
384 Release from presynaptic projections subsequently induces clustering of postsynaptic
385 molecules, initiating postsynaptic maturation.[85,90-93] Indeed, postsynaptic receptor clustering
386 was previously predicted *in silico* to increase mPSC amplitude 1.5-fold, similar to what we
387 found *in vitro*[94].
388 Thirdly, although proteomic changes plateau after 8 WPI, both synapse number and
389 synaptic strength continue to increase. Possibly, the *AZ, SV* and *presynaptic membrane* proteins
390 that are upregulated until 8 WPI are sufficient to support synapse formation thereafter.
391 Structural rearrangement and posttranslational modification of synaptic proteins, mediated
392 by e.g. ERK, PKC, PKA, CaMKII and/or RhoA/ROCK signalling[95-109], could enhance synaptic
393 strength without proteomic changes. Such processes modulate many pre- and postsynaptic
394 proteins, including gephyrin[98-100,107,110], GABA-receptors[101-105,108-110], synapsins[96,106] and
395 microtubules and their associated proteins.[110-115] Additionally, synaptic strength could be
396 regulated by (trans-synaptic) alignment of functionally related proteins in nanodomains and
397 nanocolumns, enhancing their cooperative interactions.[94,116-122] Of the few proteins that were
398 upregulated – or for the first time detected – in PB-AD neurons at 10 WPI (Supplementary
399 table 1), we found several cell adhesion molecules (CAMs) (CNTNAP4, SLITRK1, CDH1, EPHA7,
400 ITGB3, NPTX2, ITGA2, ELFN1, IGSF8 and CNTNAP1).[3,123-131], extra cellular matrix (ECM)
401 proteins (TNC and RELN)[132,133], and proteins involved in receptor clustering (NPTX2, SLITRK1,
402 PRRT1, ELFN1)[134-137] Some of which are known to strengthen GABAergic transmission.[123,126]
403 To summarize, during early development, synaptic maturation and strengthening in iPSC-
404 derived neurons coincides with increased expression of presynaptic proteins compared to
405 their postsynaptic counterparts. At later stages, further strengthening may result from
406 alignment and reorganization of the pre- and postsynaptic compartments.

407 *A versatile in vitro model for studying the role of inhibition in brain disease*
408 Dysfunction of inhibitory neurons and E/I disbalance are common aspect of
409 neurodevelopmental and neurodegenerative disorders.[5,138-143] Given the pure GABAergic
410 nature of cultures produced with the PB-AD protocol, neurons generated with this method
411 provide a versatile model to study the role of inhibition and E/I disbalance in these disorders
412 using a human, and patient-own, genetic background. Compared to a safe harbor approach,
413 our method is directly applicable to patient derived iPSCs, which makes it time and cost
414 efficient, and prevents the introduction of clonal gene editing effects. The reliable production
415 of GABAergic autaptic cultures allows for a detailed assessment of interneuron synaptic
416 properties, such as priming, fusion and synaptic plasticity in patient cell lines.[144-146]
417 Application to disease-lines will be important steps to substantiate the full potential of this
418 method. To this end, PB-AD neurons can be mixed with NGN2 neurons at defined ratios,
419 enabling accurate modelling of E/I networks at any ratio, including those found in the human
420 brain.[36-38]
421
422 **Methods**
423
424 Extended methods are available in the supplementary material.

425 *IPSC culture and delivery of transgenes*
426 IPSC's were maintained on Matrigel- or Geltrex coated-dishes in Essential 8 medium. For viral
427 induction, viral particles encoding rTTa, Ascl1, and Dlx2 were added to IPSCs and antibiotic
428 selection was performed 24 hours after transfection. For PiggyBac based strategies, IPSCs
429 were seeded as single cells after which transfection with PiggyBac transposon and
430 transposase plasmids was performed using Lipofectamine STEM. Selection was performed
431 24 hours post-transfection.

432 *Neuronal induction*
433 Transgene-selected IPSCs were seeded in N2 medium with doxycycline to induce transgene
434 expression. After 2 days of transgene expression, selection for postmitotic cells was
435 performed with antimitotic agents FUDR or AraC, and cells were collected and replated on
436 rat astrocytes in neurobasal medium supplemented with neurotrophic factors, in which
437 neurons were maintained.

438 *Electrophysiology*

Whole-cell voltage clamp was performed to measure synaptic release. For GABA puffs, perforated patch was performed, maintaining cell intrinsic chloride levels. GABAergic and glutamatergic currents were blocked with picrotoxin and DP-V + DNQX, respectively.

Immunocytochemistry and morphological analysis

Methanol- or PFA-fixed neurons were stained for MAP2, VGAT, VGLUT1/2, NEUN and Parvalbumin. After confocal microscopy analysis was performed in SynD[147] and ImageJ.

Statistics of electrophysiological and morphological data

Statistical testing was performed in Matlab and GraphPad Prism. Developmental trajectories were tested using nonparametric Spearman correlations. For timepoint comparisons, Kruskal-Wallis ANOVAs with Dunn's correction were performed. GABA puff responses were fitted using a first-order polynomial linear fit and an extra sum-of-squares F-test was employed.

Mass spectrometry

Cells were scraped, pelleted, and stored at -80°C. Sample were prepared using adapted DNA micro spin column suspension trapping protocol.[148] Pellets were extracted in SDS buffer and proteins were isolated and trypsin-digested. Peptides were eluted from the column and samples were analysed using liquid chromatography MS.

Spectra were mapped to *in silico* spectral library based on the uniprot human reference proteome peptides using DIA-NN 1.8.1.[149] Protein abundances were quantified using differential abundance analysis (DAA) of MS-DAP 1.0.5.[150] Proteins (nearly) exclusive to one group were analysed using MS-DAP differential detection (DD) test. The DEqMS[151] algorithm was used for statistical analysis and resulting p-values were adjusted using Benjamini–Hochberg False Discovery Rate (FDR) adjustment. DAA and DD results were merged. Gene set enrichment analyses were performed using GOAT online v1.0.2.[152] and SynGO knowledgebase v1.2.[153]

Cell type-associated proteomic changes were identified by expression weighted cell type enrichment (EWCE) analysis[41], based on snRNA-sequencing data derived from human cortex.[40] For cell population classifications we used cell class (e.g., GABAergic neurons) and subclass (e.g. SST^+ interneurons). Cell type-specificity scores (CTSS) for each gene were used to assign cell type labels.

Acknowledgements

The authors thank Robbert Zalm and Ingrid Saarloos for their help with cloning and plasmid production, Lisa Laan and Desiree Schut for preparation of glia feeder plates, Judith Huijgen and Solange Lopes Cardozo for preparation and maintenance of iPSCs, and Berna Özer and Remco Klaassen for performing mass-spectrometry proteomics.

This work was supported by the following grants (ZonMW-TOP BECAUSE (91216064), to M.V and L.N.C. ZonMW-PSIDER Brainmodel (10250022110003) to M.V and L.N.C., NWO-Dutch Research Agenda (NWA) NewTDec (1160.18.200) to M.V and L.N.C.), NWO Gravitation program grant BRAINSCAPES (NWO 024.004.012) to M.V. and ZonMW-OPEN (9120232310098) from the Netherlands Organisation for Scientific Research (NWO) to M.V. and L.N.C.

Declaration of interest

The authors declare no competing interests.

Author contributions

M.E.W., and J.M.C.M. designed and produced the PiggyBac construct

T.W.v.V, M.A.v.B., K.I.M., R.F.T., A.B.S., R.E.v.K, M.V. and L.N.C. designed the experiments

T.W.v.V, M.A.v.B. and J.S. performed and maintained neuronal inductions and cultures

T.W.v.V M.A.v.B. performed the patch-clamp experiments with contributions of J.S. to Fig. 1 and C.F. to Fig. S2

T.W.v.V, M.A.v.B.,. performed the immunocytochemistry experiments with contributions of J.S to Fig. 1

K.I.M., and F.K. performed the proteomics experiments and analysis

T.W.V.V, M.A.v.B., K.I.M., R.E.v.K, M.V. and L.N.C. designed figures and wrote the manuscript with input from all authors.

Supplementary information

Supplementary information will be made available with the manuscript.

Extended Methods

Key resources table

REAGENT or RESOURCE	SOURCE	IDENTIFIER
Antibodies		

MAP2	Merck Millipore	(Millipore Cat# AB5543, RRID:AB_571049)
VGAT	Synaptic Systems	(Synaptic Systems Cat# 131 002, RRID:AB_887871)
VGLUT1	Antibodies Inc.	(Antibodies Incorporated Cat# 75-066, RRID:AB_2187693)
VGLUT2	Antibodies Inc.	(Antibodies Incorporated Cat# 75-067, RRID:AB_2239153)
NeuN	Merck Millipore	(Millipore Cat# ABN78, RRID:AB_10807945)
Parvalbumin	Synaptic Systems	(Synaptic Systems Cat# 195 004, RRID:AB_2156476)
Bacterial and virus strains		
FUW-TetO-*Ascl1*-T2A-puro	Addgene	RRID:Addgene_973 29
FUW-TetO-*Dlx2* -IRES-hygro	Addgene	RRID:Addgene_973 30
FUW-M2rtTA	Addgene	RRID:Addgene_203 42
Deposited data		
PRIDE dataset " One-step induction of human GABAergic neurons promotes presynaptic development & synapse maturation"	This study	PXD064163
Transcriptomic cytoarchitecture reveals principles of human neocortex organization	Jorstad, et al.[40]	RRID:SCR_016152
Experimental models: Cell lines		
BiONI010-C-10	EBiSC	RRID:CVCL_RM84
BioNi010-C-13	EBiSC	RRID:CVCL_RF90
Kolf2.1J	Jackson Laboratory	RRID:CVCL_B5P3
GM23973	Coriell	RRID:CVCL_BW42
Recombinant DNA		
PB-TO-ASCL1-DLX2	This study	RRID:Addgene_182 307
Transposase	This study	N/A
Software and algorithms		

DIA-NN 1.8.1	Demichev, et al (2020,2022)[154,155]	
MS-DAP 1.0.5	Koopmans, et al. 2023[150]	
DEqMS	Zhu, et al, 2020[151]	
GOAT	Miedema, et al. 2022[152]	
SynGO	Koopmans, et al. 2019[153]	

iPSCs origin and culture

Unless stated otherwise, the BiONi010-C-10 stem cell line (EBISC, RRID:CVCL_RM84) was used for all experiments in this study. For glutamatergic induction, a gene-edited variant of the same line containing an integrated NGN2-casette was used (EBISC, RRID:CVCL_RF90). As a genetically independent control the KOLF2.1J (JAX, JiPSC1000, RRID:CVCL_B5P3) and GM23973 (Coriell, RRID:CVCL_BW42) lines were used. All iPSCs were maintained on Matrigel (Cornig) or Geltrex (Fisher Scientific)-coated dishes in Essential 8 (Gibco) or Essential 8 Flex (Gibco) medium and passaged with EDTA and replated in the culture medium supplemented with ROCK inhibitor Y27632 (5 µM, Tetu bio).

Lentiviral infection

Ultrahigh titre lentiviral particles were generated by Alstem (Richmond, CA, USA) from FUW-M2rtTA (Addgene, #20342, RRID:Addgene_20342), FUW-TetO-*Ascl1*-T2A-puro (Addgene #97329, RRID:Addgene_97329), and FUW-TetO-*Dlx2* -IRES-hygro (Addgene #97330, RRID:Addgene_97330). For *Ascl1*+Forskolin, iPSCs were infected with only FUW-M2rtTA and TetO-*Ascl1*-Puro, for *Ascl1* + *Dlx2* induction, iPSCs were infected with all three lentiviruses. For both lentiviral induction methods, 24 hours after infection, puromycin (1 µg/ml) selection was performed. For lentiviral *Ascl1* + *Dlx2* induction, additional hygromycin (75 µg/ml) selection was performed. For both selection regimes an uninfected control well was included to confirm successful selection before proceeding towards induction.

PiggyBac transfection

A more detailed protocol is found at the end of this document, see protocol 1. To prepare for PiggyBac transfection, iPSCs were released with accutase and plated as single cells on a Matrigel-coated 6-well plate in E8 + ROCK Inhibitor Y27632 at a density of 1500k per well. Cells were placed in the incubator to adhere for 1 to 2 hours. A total of 3 µg of DNA containing

526 the *Ascl1* + *Dlx2* PiggyBac transposon (Presented here; available on Addgene, 182307,
527 RRID:Addgene_182307) and transposase constructs (extended data 1) at a 1:3 molar ratio
528 was prepared in 100 µL of opti-MEM (GIBCO, 31985062). To another 100 µL op opti-MEM 5
529 µL of Lipofectamine STEM (Invitrogen, STEM00001) was added. Opti-MEM preparations were
530 quickly mixed by pipetting, after which the mixture was incubated at RT for 15 to 30 minutes
531 during which cells received fresh E8 + ROCK Inhibitor Y27632 to wash away non-adherent
532 cells. The opti-MEM solution was then added to the cells in a dropwise fashion. 24 hours
533 post transfection, selection with puromycin (1 µg/ml) was initiated to select only for cells
534 containing the transposon, and selection was repeated every 3-7 days.

535 *PB-AD GABAergic neuronal induction*

536 A more detailed protocol is found at the end of this document, see protocol 2. PB-AD positive
537 iPSCs were released with Accutase (Merck) on day post induction (DPI) 0 and replated with
538 at an approximate density of 3.500 cells/cm^2 in N2 medium (DMEM/F12 medium, Life
539 technologies) containing Glutamax (200 mM, Life Technologies), dextrose (0.3%, Life
540 Technologies) N2 supplement B (StemCell Technologies), Pen/Strep (0.1%, Gibco), ROCK
541 inhibitor Y27632 (10 µM, Tetubio) and doxycycline hyclate (2 µg/mL) onto Matrigel (Cornig)
542 or Geltrex (Fisher Scientific) coated dishes. On DPI 1, medium was refreshed using the same
543 composition without ROCK inhibitor Y27632. On DPI 2, the medium was refreshed once more
544 with the same composition as on DPI 1, with the addition of 5-Fluoro-2'-deoxyuridine (FUDR)
545 (10 µM, Sigma-Aldrich) or Cytosine β-D-arabinofuranoside (AraC, 20 µM, Sigma-Aldrich) to
546 remove proliferative cells. On DPI 3, neurons were released with accutase, pelleted, and
547 resuspended and plated in Neurobasal medium (Life Technologies) supplemented with
548 Glutamax (200 mM), B27 (0.1%) Pen-Strep (0.1%), fetal bovine serum (0.5%), BDNF (10 ng/ml,
549 Peprotech), CNTF (10ng/ml, Peprotech), GDNF (10 ng/ml, Peprotech) and doxycycline hyclate
550 (2 µg/mL; Sigma-Aldrich). Neurons were plated to the required respective preparations (see
551 *Autaptic culture* and *Network culture*).

552 *Glutamatergic neuronal induction*

553 For glutamatergic induction, Bioni010-C-13 iPSCs were released with Accutase (Merck) on
554 DPI 0 and replated with at an approximate density of 3.500 cells/cm^2 in N2 medium
555 (DMEM/F12 medium, Life technologies) containing Glutamax (200 mM, Life Technologies),
556 dextrose (0.3%, Life Technologies) N2 supplement B (StemCell Technologies), Pen/Strep
557 (0.1%, Gibco) and doxycycline hyclate (2 µg/mL; Sigma-Aldrich) combined with dual-SMAD
558 inhibitors LDN193189 (100 nM, Stemgent), SB431542 (10 µM, Tocris Bioscience), and XAV939
559 (2 µM, Stemgent) NT3 (10 ng/ml, Peprotech) and doxycycline hyclate (2 µg/mL) onto Matrigel

560 (Cornig) or Geltrex (Fisher Scientific) coated dishes. On DPI 1, medium was refreshed using
561 the same composition without ROCK inhibitor Y27632. On DPI 2, the medium was refreshed
562 once more with the same composition as on day 2, with the addition of 5-Fluoro-2'-
563 deoxyuridine (FUDR) (10 μM, Sigma-Aldrich) or Cytosine β-D-arabinofuranoside (AraC, 20 μM,
564 Sigma-Aldrich) to remove proliferative cells. On DPI 3, neurons were released with accutase,
565 pelleted, resuspended and plated in Neurobasal medium (Life Technologies) supplemented
566 with Glutamax (200 mM), B27 (0.1%) Pen-Strep (0.1%), foetal bovine serum (0.5%), BDNF (10
567 ng/ml, Peprotech), CNTF (10ng/ml, Peprotech), GDNF (10 ng/ml, Peprotech) and doxycycline
568 hyclate (2 μg/mL; Sigma-Aldrich). Neurons were plated to the required respective
569 preparations (see *Autaptic culture* and *Network culture*).

570 *Lentiviral GABAergic induction*

571 In general, lentiviral GABAergic induction protocols followed a similar workflow as PB-AD
572 induction. To better adhere to established protocols.[14,15], the medium composition differed at
573 certain steps (Figure 1H). For Ascl1 + Forskolin induction, from DPI 0 onwards, Forskolin (10
574 μM, Merck) was added to the medium up to DPI 14. Furthermore, from DPI0 onwards non-
575 essential amino acids (1:100, Sigma) were added up to day DPI 14. BDNF (10 ng/ml) and NT3
576 (10 ng/ml) were present from DPI1 onwards. For lentiviral *Ascl1* + *Dlx2* induction BDNF (10
577 ng/ml) and NT3 (10 ng/ml) were added from DPI 0 onward, as well. Furthermore, laminin
578 (1μg/ml, Sigma-Aldrich), cyclic AMP (1 μM, Sigma-Aldrich), and Ascorbic Acid (200 μM, Sigma-
579 Aldrich), were added to the medium at all subsequent refreshments to improve viability.

580 *Autaptic culture*

581 Neurons were plated at a density of ~ 400 cells / cm^2 on micro-islands prepared from rat
582 glial cells plated on agarose-coated coverslips stamped with a custom stamp in Poly-D-
583 Lysine (0.1 mg/ml, Sigma), rat tail collagen (0.7 mg/ml, Corning) and Fibronectin (100 μg/ml,
584 Corning) in acetic acid (10 mM, sigma). Glial islands were prepared approximately 7 days
585 before plating neurons and were treated with AraC (20 μM, Sigma-Aldrich) before plating
586 neurons. Autaptic cultures were refreshed every 7 days with a ~50% media refreshment, with
587 the same medium as used for plating neurons, but omitting doxycycline hyclate (except for
588 Figure 1E-G, where doxycycline hyclate was added up to DPI 14).

589 *Network culture*

590 Neurons were plated at a density of ~ 7000 cells / cm^2 on coverslips covered with a glial-
591 monolayer prepared from rat astrocytes a week in advance and treated with Cytosine β-D-
592 arabinofuranoside (20 μM, Sigma-Aldrich) 24-48 hours before plating neurons. Networks

593 cultures were refreshed with a ~50% media refreshment every 3-4 days, with the same
594 medium as used for plating neurons, but omitting doxycycline hyclate.

595 *Electrophysiology*

596 Whole-cell voltage-clamp recordings ($V_m = -70$ mV) were performed on autaptic neurons,
597 with borosilicate glass pipettes (2 – 5MΩ) filled with (in mM) 136 KCl, 17.8 HEPES, 1 EGTA,
598 0.6 $MgCl_2$, 4 ATP-Mg, 0.3 GTP-Na, 12 phosphocreatine-K_2 and 50 units/mL phosphocreatine
599 kinase (pH = 7.30, 290 mOsmol). The external solution contained in mM: 10 HEPES, 10
600 glucose, 140 NaCl, 2.4 KCl, 4 $MgCl_2$, and 4 $CaCl_2$ (pH = 7.30, 290 mOsmol). Experiments were
601 performed at room temperature (~22°C using a MultiClamp700B amplifier (Axon
602 Instruments) and Digidata 1440A digitizer under control of Clampex 10 software (Molecular
603 devices). Only cells with an access resistance < 15MΩ (80% compensated) and leak current
604 of <300 pA were included. Synaptic responses were elicited by 0.5 ms depolarization to
605 30 mV.

606 For GABA puffs, perforated patch recordings were produced by filling the patch pipette
607 (in mM) 140 KCl, 10 HEPES, gramicidin (100 µg/ml) and allowing cells to perforate for 15-30
608 minutes after reaching a GΩ seal to < 100 MΩ series resistance. Puff pipettes filled with 100
609 µM GABA in ACSF were positioned near the soma, at approximately 25 µm distance. 100 ms
610 puffs were applied at -110, -90, -70, -50, -30 and -10 mV holding voltages to induce GABAergic
611 currents. Cells were discarded if a sudden swift decrease in resistance was observed during
612 perforation, or if the observed reversal potential of Cl^- was ± 0 mV, which indicates exchange
613 of the patch-pipette solution with the intracellular solution.

614 *Electrophysiology; pharmacology*

615 To Block GABA-currents, picrotoxin (100 µM, Hello Bio) was used. A 100 mM stock was
616 prepared in DMSO and was added to the bath to reach the final concentration. To block
617 glutamatergic currents, AP-V (100 µM, R&D systems) and DNQX (40 µM, Tocris) were used.
618 For DNQX, A 1000x of stock of each was prepared in DMSO. For AP-V, the stock was prepared
619 in water.

620 *Electrophysiology; analysis electrophysiological data.*

621 Offline analysis was performed using custom-written programs[156] in Matlab (Mathworks).
622 Experimental conditions were blinded during analysis. In all figures, stimulation artefacts
623 have been removed. For evoked release during 20 Hz stimulation, back-extrapolation of
624 linear fits from the last 20 pulses of the cumulative charge was used to estimate the RRP (y-
625 intercept).[157]

Immunocytochemistry and morphological analysis

Neurons were fixed in ice cold 100% methanol (VWR) for 15 minutes at 4°C, blocked with 2.5% normal goat serum (NGS, Life Technologies) and 0.1% Triton X-100 in PBS for 45 minutes and incubated with primary antibodies in PBS with 2.5% NGS and 0.1% Triton X-100 overnight at 4°C. The following primary antibodies were used: chicken anti-MAP2 (1:1000, Merck AB5543, RRID:AB_571049); rabbit anti-VGAT (1:2000, SySy #131 002, RRID:AB_887871), mouse anti-VGlut1 (1:250, NeuroMab clone N28/9, Antibodies inc. 75-066, RRID:AB_2187693), mouse anti-VGlut2 (1:250, NeuroMab clone N29/29, Antibodies inc. 75-067, RRID:AB_2239153). For Rabbit anti-NeuN (1:500, Merck ABN78, RRID:AB_10807945) and anti-Parvalbumin (1:500, SySy #195 004, RRID:AB_2156476) staining neurons were fixed with 3.7% PFA for 15 minutes at room temperature, instead of methanol fixation. After washing with PBS the next day, cells were incubated for 1 h at room temperature with secondary antibodies conjugated to Alexa dyes (1:1000, Invitrogen Molecular Probes), washed again and mounted with DABCO-Mowiol (Invitrogen). Images were acquired at 1024x1024 pixels on a Nikon Eclipse Ti confocal laser scanning microscope (40× objective; NA 1.3) with NIS-Elements software. Z-stacks were produced at a 0.5 µm step-size until no more puncta and/or dendrites were in focus. Confocal settings were kept constant for all scans within an experimental week. Analysis of neuronal morphology was performed on maximum-intensity projections using the automated image analysis routine SynD.[147] for autaptic neurons and a custom ImageJ workflows for network analysis, in either case, for VGAT and VGLUT puncta counts, only puncta on dendrites were counted.

Statistics of electrophysiological and morphological data

Statistical testing was performed in MATLAB and GraphPad Prism For descriptive statistics (Figure 1) the likelihood of normality vs lognormality was calculated, which revealed that the data was lognormally disturbed. Therefore the geometric mean and geometric SD factor were calculated and reported. In autaptic development timelines (Figure 4&5), no data was normally distributed. Therefore, to test general developmental trajectories, nonparametric Spearman correlations were computed with a two-tailed test for significance and a 95% confidence interval. For timepoint comparisons, Kruskal-Wallis ANOVAs were performed with Dunn's multiple comparisons test. Pairwise comparisons were made between 4 and 6, 6 and 8, and 8 and 10 WPI. #, ##, ###, #### and *ns* represent results of spearman correlation results, *, **, ***, **** and ns represent Kruskal-Wallis ANOVA results. *ns* and ns represent non-significant results. Single, double, triple and quadruple marks represent (corrected) $p < 0.05$, $p < 0.01$, $p < 0.001$ and $p < 0.0001$, respectively. GABA-puff responses (figure 6O) were fitted

using a first-order polynomial linear fit and an extra sum-of-squares F-test was used to determine whether GABA responses were identical throughout development. In plots, unless stated otherwise, the lines in boxplots represent the median value. Crosses represent the mean value. Boxes represent 50% off the values. Circular markers represent individual observations. Quantifications are available in the supplementary data, and each figure contains n (number of cells) and N (number of inductions) values per parameter in either the relevant graph or typical example.

Mass spectrometry; Cell pellet harvesting for MS

Cells were washed three times with 1 ml sterile Dulbecco's PBS (Gibco), whereof first twice at 37°C and finally once at 4 °C. Cultures were kept on ice, scraped off using VWR cell lifters, and harvested in 1.5 ml protein LoBind Eppendorf tubes (VWR). Pellets were obtained by centrifugation at 1,000 × g for 5 minutes at 4 °C. Supernatant was removed and pellets were kept at -80 °C before subsequent sample preparation.

Mass spectrometry; MS sample preparation

MS sample preparation was performed following the DNA micro spin column suspension trapping protocol[148], with some minor adaptations. Cell pellets were extracted and reduced in 6% SDS buffer, containing 50 mM Tris-HCl (pH 8) and 5 mM tris (2-carboxyethyl)phosphine (TCEP), by incubation at 55°C for 15 minutes in a thermomixer set to 1400 RPM. Free sulfhydryl groups were alkylated by incubation with 20 mM methyl methanethiosulfonate (MMTS; 200 mM stock solution) for 15 minutes at RT. Insoluble debris was cleared by centrifugation at 10000g for 1 minute at RT and the supernatant was transferred to a new tube (Eppendorf). Next, samples were acidified by addition of 1.1% phosphoric acid (12% stock solution), mixed with six volumes of binding/washing buffer (90% methanol and 100mM Tris-HCl, pH 8) and loaded onto a plasmid DNA micro column (HiPure from Magen Biotechnology). The protein particulate was retained on the column upon centrifugation at 1400x g for 1 minute and the columns were washed four times with binding/washing buffer. Columns were transferred to a new tube (Eppendorf), supplemented with 500 ng Trypsin/Lys-C (Promega) in 50 mM NH4HCO3 and incubated overnight at 37°C in a humidified incubator. Tryptic peptides were eluted and pooled by subsequent addition of 50 mM NH4HCO3, 0.1% formic acid and 0.1% formic acid in acetonitrile. Collected peptides were dried by SpeedVac and stored at -80°C.

Mass spectrometry; LC-MS Analysis

692 Each sample of tryptic digest was redissolved in 0.1% formic acid and the peptide
693 concentration was determined by tryptophan-fluorescence assay[158]; 75 ng of peptide was
694 loaded onto an Evotip Pure (Evosep). Peptide samples were separated by standardized 30
695 samples per day method on the Evosep One liquid chromatography system, using a 15 cm ×
696 150 µm reverse-phase column packed with 1.5 µm C18-beads (EV1137 from Evosep)
697 connected to a 20 µm ID ZDV emitter (Bruker Daltonics). Peptides were electro-sprayed into
698 the timsTOF Pro 2 mass spectrometer (Bruker Daltonics) equipped with CaptiveSpray source
699 and measured with the following settings: Scan range 100-1700 m/z, ion mobility 0.65 to
700 1.5 Vs/cm2, ramp time 100 ms, accumulation time 100 ms, and collision energy decreasing
701 linearly with inverse ion mobility from 59 eV at 1.6 Vs/cm2 to 20 eV at 0.6 Vs/cm2. Operating
702 in dia-PASEF mode, each cycle took 1.38 s and consisted of 1 MS1 full scan and 12 dia-PASEF
703 scans. Each dia-PASEF scan contained two isolation windows, in total covering 300-1200 m/z
704 and ion mobility 0.65 to 1.50 Vs/cm2. Dia-PASEF window placement was optimized using the
705 py-diAID tool[159] Ion mobility was auto calibrated at the start of each sample (calibrant m/z,
706 1/K0: 622.029, 0.992 Vs/cm2; 922.010, 1.199 Vs/cm2; 1221.991, 1.393 Vs/cm2).

707 *Mass spectrometry; MS data Analysis*

708 DIA-PASEF raw data were processed with DIA-NN 1.8.1.[154,155] An in-silico spectral library was
709 generated from the uniprot human reference proteome (SwissProt and TrEMBL, canonical
710 and additional isoforms, release 2023-2) using Trypsin/P digestion and at most 1 missed
711 cleavage. Fixed modification was set to beta-methylthiolation (C) and variable modifications
712 were oxidation (M) and N-term M excision (at
713 most 1 per peptide). Peptide length was set to 7-30, precursor charge range was set to 2-4,
714 precursor m/z was limited to 280–1220, both MS1 and MS2 mass accuracy were set to 15
715 ppm, scan window was set to 9, double-pass-mode and match-between-runs were enabled.
716 Protein identifiers (isoforms) were used for protein inference. All other settings were left as
717 default.

718 MS-DAP 1.0.5.[150] was used for downstream differential abundance analyses using the
719 DIA-NN results. Filtering and normalization was applied to respective samples per statistical
720 contrast. Peptide-level filtering was configured to retain only peptides identified in at least
721 4 samples in both experimental conditions (within current contrast) and only proteins with
722 2 valid peptides were retained. Next, peptide abundance values were normalized by
723 minimizing the mode $\log_2$ (FC) between sample pairs (MWMB algorithm), followed by
724 protein-level mode-between normalization. The DEqMS[151] algorithm was used for statistical
725 analysis and resulting p-values were adjusted for multiple testing using the Benjamini–

726 Hochberg False Discovery Rate (FDR) procedure. To investigate proteins with strong
727 differences in detection rates between conditions, e.g. consistently detected in one condition
728 but (near) absent in another, the MS-DAP differential detection test was applied to all
729 proteins that were observed with at least 2 peptides in at least 4 samples in either condition
730 (i.e. confidently detected proteins). Using the default MS-DAP workflow, we merged
731 differential detection (DD) results into the DEqMS result table for the subset of proteins that
732 had both an absolute DD z-score of at least 6 and a smaller adjusted p-value in DD (or no p-
733 value from DEqMS due to a lack of data points in either condition).

734 *Mass spectrometry; Expression-weighted cell type enrichment analysis*

735 Cell type enrichment analysis gives insight into the cell types that potentially drive
736 differential expression. EWCE uses single-cell RNA-sequencing data to generate a probability
737 distribution associated with a gene list having an average level of expression within a cell[41]
738 Although it's based on RNA expression levels, it can also be applied to proteomics data.[160]
739 We used published single nucleus RNA-sequencing data (49,495 nuclei) from human cortical
740 brain regions – including middle temporal gyrus, anterior cingulate cortex, primary visual
741 cortex, primary motor cortex, primary somatosensory cortex and primary auditory cortex –
742 published by Jorstad et al.[40] For cell type annotations we used the cell type annotations: class
743 (e.g., GABAergic neurons) and subclass (e.g. SST^+ interneurons) for first and second level
744 EWCE analysis, respectively. Bootstrap enrichment tests were performed using 10,000 reps
745 to look whether gene sets (i.e., foreground) were significantly enriched for a cell class or
746 subclass relative to the background (i.e., all detected proteins included in that contrast). Since
747 we focused on neuronally-enriched proteins or SYNGO-annotated synaptic proteins, we
748 excluded non-neuronal enrichment scores.

749 EWCE calculates cell type-specificity scores (CTSS) for all genes, which is the
750 percentage of mean expression per cell type relative to the sum of the mean expressions of
751 all cell types. We used the CTSS to predict for each protein the cell type the protein probably
752 is derived from. We only included CTSS from genes that passed mRNA detection threshold
753 (mean expression >4 in at least one cell class). Cell type predictions included neuronal
754 (neuronal CTSS > 70%), GABAergic neurons (GABA CTSS > 0.8 and glutamatergic CTSS < 0.1),
755 glutamatergic neurons (glutamatergic CTSS > 0.8 and GABAergic CTSS < 0.1). Cell type
756 predictions were labelled in volcano plots. We also used the EWCE-calculated mean mRNA
757 expression for each cell type to estimate the differential expression of genes in GABAergic
758 vs glutamatergic neurons, which was used in the SYNGO manual colour plots (Figure 6H)).

759 *Mass spectrometry; Heatmaps and line plots*

760 We used the mean log_2-transformed normalized protein intensities per group (i.e., PBAD 4
761 WPI) and plotted these values using line plots in RStudio.[161] using ggplot[162] The relative
762 normalized protein intensities (log_2 (FC)) was used in heatmaps, which were produced using
763 Morpheus. To map these proteins to predicted cell types we also show EWCE-calculated cell
764 type specificity scores. All heatmaps visualizations are with fixed colour scaling (i.e., not
765 relative colour scaling per gene), as indicated by heatmap legend.

766 *Mass spectrometry; Gene-set enrichment analysis using GOAT and over-representation analysis*
767 *using SYNGO*
768 We used the output of the differential abundance analysis using MSDAP (PB-AD 10 vs 4 WPI
769 and NGN2 10 vs 4 WPI) as input for gene-set enrichment analysis using GOAT. The GOAT
770 online v1.0.2.[152] was used to perform gene set enrichment analyses using gene sets from the
771 SynGO knowledgebase v1.2[153] Effect size-derived gene scores (i.e., log_2 (FC)) were used to
772 test for enriched gene sets that contained at least 10 and at most 1500 genes (or 50% of the
773 gene list, whichever was smaller) that overlapped with the input gene list. Multiple testing
774 correction was independently applied per gene set "source" (i.e. SYNGO_CC, SYNGO_BP) using
775 Bonferroni adjustment and all p-values were again adjusted using Bonferroni correction to
776 account for 2 separate tests across "sources". The significance threshold for adjusted p-values
777 was set to 0.05. SYNGO over-representation analysis was performed using the same MSDAP
778 output. Foreground was defined as upregulated proteins per contrast (p-adjusted < 0.05 and
779 log_2 (FC) > 0.1), and the background contained all tested genes for that contrast. SynGO
780 release is dataset version: 20231201, and default settings were used. Ontologies are
781 significantly enriched at 1% FDR, while including terms containing at least three matching
782 input genes.

783 *Protocol 1: PiggyBac transfection*
784 *Introduction*
785 In this protocol it is described how IPSCs are transfected with the transposon and
786 transposase to allow for neuronal induction of PB-AD neurons.
787 *Materials*
788 - Geltrex (Cornig) or Matrigel (Fisher Scientific)
789 - Essential 8 (Gibco) or Essential 8 Flex (Gibco)
790 - Accutase (Millipore; SCR005)
791 - DMEM-F12 (Life technologies)
792 - opti-MEM (GIBCO, 31985062)
793 - Lipofectamine STEM (Invitrogen, STEM00001)

794 • Rock Inhibitor Y27632 (Tetu-Bio, T1725) or CEPT cocktail (chroman 1 (Mechem
795 Expresss, HY-15392), emricasan (Selleckchem, S7775), polyamine (Sigma, P8483),
796 and trans-ISRIB (Tocris, 5284))
797 • Doxycycline hyclate 2 µg/mL (Sigma, D9891)
798 • Puromycin (Sanbio, 13884-25)
799 • Piggybac transposase (see supplementary plasmid map)
800 • *Distribution of the transposase through Addgene is not possible. We advise*
801 *synthesis inhouse or commercially using the supplied plasmid map.*
802 • *Ascl1* + *Dlx2* PiggyBac transposon (Addgene, 182307, RRID:Addgene_182307)
803 *Protocol*
804 • Coat your plates with Geltrex or Matrigel according to manufacturer instructions.
805 Culture IPSCs in 1x6w until 70-90% confluent.
806 • Prepare a fresh coated 1x6w for plating infected cells. Prewarm Essential 8 or
807 Essential 8 Flex + Rock Inhibitor Y27632 (RI, 10 µm) or CEPT (50 nM, 5 µM, 1x, 07.
808 µM respectively).
809 • *Some IPSC lines are more easily transfected then others. If severe cell-death or*
810 *bad transfection efficiency are observed, CEPT cocktail can improve this.*
811 • Aspirate the medium of the IPSCs and wash 1x with PBS.
812 • Aspirate medium and add 350 µl accutase to 1x6w IPSCs. Incubate at 37 °C For
813 approx. 5-10 minutes or until cells detach.
814 • Meanwhile, aspirate the coating medium from a new plate and add Essential 8 or
815 Essential 8 Flex + RI or CEPT.
816 • Once cells have detached, collect cells with 4.5 ml DMEM + RI and spin down 5
817 minutes at 1000 RPM / 180 RCF.
818 • Aspirate the supernatant and resuspend cells in 1 ml of Essential 8 or Essential 8
819 Flex + RI or CEPT cocktail.
820 • Count cells and plate 1000 to 1500k cells per 1x6w well, 500 to 750k cells per
821 1x12w or 200 to 300k per 1x24w.
822 • Let cells adhere for 1 to 2 hours at 37 °C/5% CO_2.
823 • Per transfection, prepare the mixes as stated in table 1. Give the Opti-MEM a few
824 minutes to warm to RT before adding the other components to each mix.

825 *Table: Mixing ratio for transfection of piggyBac constructs*

6 well			**12 well**			**24 well**		
	Mix 1	**Mix 2**		**Mix 1**	**Mix 2**		**Mix 1**	**Mix 2**
Opti-MEM	100 µl	100 µl	**Opti-MEM**	50 µl	50 µl	**Opti-MEM**	20 µl	20 µl
DNA	3 µg		**DNA**	1.5 µg		**DNA**	0.6 µl	
Lipofectamine stem		5 µl	**Lipofectamine stem**		2.5 µl	**Lipofectamine stem**		1 µl

826
827 - For DNA, mix the transposase and transposon at a molar ratio of 1:3.
828 - Combine mix 1 and 2 and mix well by pipetting up and down. Incubate transfection
829 mix for 15 to 30 minutes at RT.
830 - Replace Essential 8 or Essential 8 Flex + RI or CEPT on the cells during this
831 incubation step, to wash away any non-adherent cells and debris.
832 - Add the mixture to the cells in a dropwise fashion, evenly distributed throughout
833 the well. Immediately swirl the plate to ensure even distribution, and return plate to
834 37 °C/5% CO_2.
835 - Over the following 24 to 72 hours, BFP expression should appear. Culture cells to
836 70-90% confluency or for 1 week before splitting if confluency isn't reached.
837 - Once cells are 50-70% confluent, add puromycin for selection. This selection regime
838 can be started 48h after transfection, if cells divide quickly, or later. The required
839 concentration can vary between cell-lines. For most lines, 1 µg/ml puromycin for a
840 minimum of two days is recommended.
841 - Take along a well of untransfected IPSCs of the same genotype as a control
842 and only stop selection once no cells survive in this well.
843 - Expand selected cells and use as needed. Repeated antibiotic selection should be
844 performed weekly to ensure stable integration of the transposon is maintained.

845

846 *Protocol 2: PB-AD GABAergic neuronal induction*

847 *Materials*

848 - Matrigel (Cornig), Geltrex (Fisher Scientific)
849 - Accutase (Millipore; SCR005)
850 - Rock Inhibitor Y27632 10 μM (Tetu-Bio, T1725) (RI)
851 - Doxycycline hyclate 2 μg/mL (Sigma, D9891) (Dox)
852 - FUDR (Sigma, F0503) 10 μM **or** AraC (Sigma, C1768) 20 μM
853 - AraC more efficiently selects only postmitotic cells and is recommended, but
854 if lentiviral infection after induction is needed FUDR selection allows for
855 higher infection efficiency after selection.
856 - Neurotrophic Factors
857 - BDNF (Stemcell Technologies; 78005.3) - 10 ng/ml
858 - CNTF (Peprotech; 450-13) - 10 ng/ml
859 - GDNF (Stemcell Technologies; 78058.3) - 10 ng/ml
860 - DMEM (VWR; 392-0415P)
861 - foetal bovine serum (2%, Life Tech; 10270106)
862 - N2 Medium
863 - DMEM/F12 medium (Life Technologies)
864 - Glutamax (200 mM, Life Technologies)
865 - dextrose (0.3%, Life Technologies)
866 - N2 supplement B (StemCell Technologies)
867 - Pen/Strep (0.1%, Gibco)
868 - Neurobasal Medium
869 - Neurobasal medium (Life Technologies)
870 - Dextrose (Life Tech; A2494001) – 0.3% final concentration – use 1:67
871 - Glutamax (200 mM)
872 - NEAA (Life Tech; 11350912) - 1:200
873 - B27 (0.1%)
874 - Pen-Strep (0.1%)
875 - foetal bovine serum (Life Tech; 10270106, 0.5%)

876

877 *Protocol*

878 **Day 0: Start induction**

879 1. Per 1x6w IPSCs coat 1x 10cm dish with Geltrex or Matrigel according to
880 manufacturer instructions. Prewarm 10 ml of N2 + RI + Dox, 5 ml of DMEM + 2% FBS
881 per 1x6w to induce, and 5 ml PBS.

882 2. Remove media from IPSCs and wash 1x with warm PBS.

883 3. Add 300 µl accutase per 6-well.

884 4. Incubate for 5 minutes at 37°C.

885 5. Add 3 ml DMEM and pipet up and down to collect cells.

886 6. Pellet for 5 minutes at 1000 RPM / 180 RCF.

887 7. Resuspend pellet in 1 ml N2 medium with RI + Dox.

888 8. Plate cells as single-cells in a 10 cm dish with 9 ml N2 medium with RI + Dox.

889 **Day 1: Repeat Doxycycline and remove RI**

890 9. The following day, replace 100% of the medium with N2 + Dox

891 **Day 2: Repeat Doxycycline and select postmitotic cells**

892 10. The following day, replace 100% of the medium with N2 + Dox + FUDR **or** N2 + Dox
893 + AraC

894 **Day 3: Replate neurons to target vessel**

895 11. Prepare Neurobasal medium + DOX + CNTF + GDNF + BDNF (if using FUDR, + FUDR)

896 12. When media is warm, transfer it to prepared plates. Induced GABAergic neurons
897 thrive in co-culture with glia. Neurons can be replated to coverslips pre-seeded with
898 glia, or be mixed with glia and plated simultaneously.

899 13. Wash induced neurons 1x with PBS.

900 14. Add accutase to your induced neurons (1.5 ml in 10 cm dish).

901 15. Incubate for 5 minutes at 37°C or until cells are released.

902 16. Add 3 ml of DMEM + 2% FBS and pipette up and down to collect cells.

903 17. For 1x10 cm dish, use 13 ml of medium for collection.

904 18. Pellet cells for 5 min at 1000 RPM / 180 RCF.

905 19. Resuspend the pellet in 1 ml NBM + Dox + BDNF + CNTF + GDNF and count cells.

906 20. Plate neurons at your required density.

907 *Feeding*

908 21. Feeding rates depend on experimental conditions. For the experiments as described
909 here, low density (autaptic) cultures are fed once a week. Higher density cultures are

fed twice a week. In all cases, a ~50% medium refreshment is performed. Media composition is the same as the glia-transfer medium, but AraC/FUDR is omitted.

Material availability

PiggyBac *Ascl1-Dlx2* construct is available from Addgene #182307. The mass spectrometry proteomics data have been deposited to the ProteomeXchange Consortium via the PRIDE partner repository.[163] with the dataset identifier PXD064163.

References

1. Breschi, A., Gingeras, T.R., and Guigó, R. (2017). Comparative transcriptomics in human and mouse. Nature Reviews Genetics *18*, 425-440. 10.1038/nrg.2017.19.

2. Gharib, W.H., and Robinson-Rechavi, M. (2011). When orthologs diverge between human and mouse. Briefings in Bioinformatics *12*, 436-441. 10.1093/bib/bbr031.

3. Stachniak, T.J., Sylwestrak, E.L., Scheiffele, P., Hall, B.J., and Ghosh, A. (2019). Elfn1-Induced Constitutive Activation of mGluR7 Determines Frequency-Dependent Recruitment of Somatostatin Interneurons. J Neurosci *39*, 4461-4474. 10.1523/jneurosci.2276-18.2019.

4. Rubenstein, J.L.R., and Merzenich, M.M. (2003). Model of autism: increased ratio of excitation/inhibition in key neural systems. Genes, Brain and Behavior *2*, 255-267. 10.1034/j.1601-183x.2003.00037.x.

5. Palop, J.J., Chin, J., Roberson, E.D., Wang, J., Thwin, M.T., Bien-Ly, N., Yoo, J., Ho, K.O., Yu, G.Q., Kreitzer, A., et al. (2007). Aberrant excitatory neuronal activity and compensatory remodeling of inhibitory hippocampal circuits in mouse models of Alzheimer's disease. Neuron *55*, 697-711. 10.1016/j.neuron.2007.07.025.

6. Busche, M.A., Eichhoff, G., Adelsberger, H., Abramowski, D., Wiederhold, K.-H., Haass, C., Staufenbiel, M., Konnerth, A., and Garaschuk, O. (2008). Clusters of Hyperactive Neurons Near Amyloid Plaques in a Mouse Model of Alzheimer's Disease. Science *321*, 1686-1689. doi:10.1126/science.1162844.

7. Nelson, S., and Valakh, V. (2015). Excitatory/Inhibitory Balance and Circuit Homeostasis in Autism Spectrum Disorders. Neuron *87*, 684-698. 10.1016/j.neuron.2015.07.033.

8. Foss-Feig, J.H., Adkinson, B.D., Ji, J.L., Yang, G., Srihari, V.H., McPartland, J.C., Krystal, J.H., Murray, J.D., and Anticevic, A. (2017). Searching for Cross-Diagnostic Convergence: Neural Mechanisms Governing Excitation and Inhibition Balance in Schizophrenia and Autism Spectrum Disorders. Biol Psychiatry *81*, 848-861. 10.1016/j.biopsych.2017.03.005.

9. Sohal, V.S., and Rubenstein, J.L.R. (2019). Excitation-inhibition balance as a framework for investigating mechanisms in neuropsychiatric disorders. Molecular Psychiatry *24*, 1248-1257. 10.1038/s41380-019-0426-0.

10. Nicholas, C.R., Chen, J., Tang, Y., Southwell, D.G., Chalmers, N., Vogt, D., Arnold, C.M., Chen, Y.-J.J., Stanley, E.G., and Elefanty, A.G. (2013). Functional maturation of hPSC-derived forebrain interneurons requires an extended timeline and mimics human neural development. Cell stem cell *12*, 573-586.

11. Liu, Y., Liu, H., Sauvey, C., Yao, L., Zarnowska, E.D., and Zhang, S.-C. (2013). Directed differentiation of forebrain GABA interneurons from human pluripotent stem cells. Nature protocols *8*, 1670-1679.

12. Maroof, A.M., Keros, S., Tyson, J.A., Ying, S.-W., Ganat, Y.M., Merkle, F.T., Liu, B., Goulburn, A., Stanley, E.G., and Elefanty, A.G. (2013). Directed differentiation and functional maturation of cortical interneurons from human embryonic stem cells. Cell stem cell *12*, 559-572.

13. Engle, S.J., Blaha, L., and Kleiman, R.J. (2018). Best Practices for Translational Disease Modeling Using Human iPSC-Derived Neurons. Neuron *100*, 783-797. 10.1016/j.neuron.2018.10.033.

14. Mossink, B., van Rhijn, J.-R., Wang, S., Linda, K., Vitale, M.R., Zöller, J.E.M., van Hugte, E.J.H., Bak, J., Verboven, A.H.A., Selten, M., et al. (2022). Cadherin-13 is a critical regulator of GABAergic modulation in human stem-cell-derived neuronal networks. Molecular Psychiatry *27*, 1-18. 10.1038/s41380-021-01117-x.

15. Yang, N., Chanda, S., Marro, S., Ng, Y.H., Janas, J.A., Haag, D., Ang, C.E., Tang, Y., Flores, Q., Mall, M., et al. (2017). Generation of pure GABAergic neurons by transcription factor programming. Nat Methods *14*, 621-628. 10.1038/nmeth.4291.

16. Baum, C. (2007). Insertional mutagenesis in gene therapy and stem cell biology. Current opinion in hematology *14*, 337-342.

17. Cabrera, A., Edelstein, H.I., Glykofrydis, F., Love, K.S., Palacios, S., Tycko, J., Zhang, M., Lensch, S., Shields, C.E., Livingston, M., et al. (2022). The sound of silence: Transgene silencing in mammalian cell engineering. Cell Systems *13*, 950-973. https://doi.org/10.1016/j.cels.2022.11.005.

18. Wolf, D., and Goff, S.P. (2009). Embryonic stem cells use ZFP809 to silence retroviral DNAs. Nature *458*, 1201-1204. 10.1038/nature07844.

19. Yao, S., Sukonnik, T., Kean, T., Bharadwaj, R.R., Pasceri, P., and Ellis, J. (2004). Retrovirus Silencing, Variegation, Extinction, and Memory Are Controlled by a Dynamic Interplay of

Multiple Epigenetic Modifications. Molecular Therapy *10*, 27-36. 10.1016/j.ymthe.2004.04.007.

20. Miller, J.C., Tan, S., Qiao, G., Barlow, K.A., Wang, J., Xia, D.F., Meng, X., Paschon, D.E., Leung, E., Hinkley, S.J., et al. (2011). A TALE nuclease architecture for efficient genome editing. Nature Biotechnology *29*, 143-148. 10.1038/nbt.1755.

21. Peitz, M., Krutenko, T., and Brüstle, O. (2020). Protocol for the Standardized Generation of Forward Programmed Cryopreservable Excitatory and Inhibitory Forebrain Neurons. STAR Protoc *1*, 100038. 10.1016/j.xpro.2020.100038.

22. Schmid, B., Holst, B., Poulsen, U., Jørring, I., Clausen, C., Rasmussen, M., Mau-Holzmann, U.A., Steeg, R., Nuthall, H., Ebneth, A., and Cabrera-Socorro, A. (2021). Generation of two gene edited iPSC-lines carrying a DOX-inducible NGN2 expression cassette with and without GFP in the AAVS1 locus. Stem Cell Research *52*, 102240. https://doi.org/10.1016/j.scr.2021.102240.

23. Lombardo, A., Cesana, D., Genovese, P., Di Stefano, B., Provasi, E., Colombo, D.F., Neri, M., Magnani, Z., Cantore, A., Lo Riso, P., et al. (2011). Site-specific integration and tailoring of cassette design for sustainable gene transfer. Nature Methods *8*, 861-869. 10.1038/nmeth.1674.

24. Pi, H.-J., Hangya, B., Kvitsiani, D., Sanders, J.I., Huang, Z.J., and Kepecs, A. (2013). Cortical interneurons that specialize in disinhibitory control. Nature *503*, 521-524. 10.1038/nature12676.

25. Wilber, A., Linehan, J.L., Tian, X., Woll, P.S., Morris, J.K., Belur, L.R., McIvor, R.S., and Kaufman, D.S. (2007). Efficient and stable transgene expression in human embryonic stem cells using transposon-mediated gene transfer. Stem Cells *25*, 2919-2927. 10.1634/stemcells.2007-0026.

26. Ng, Y.H., Chanda, S., Janas, J.A., Yang, N., Kokubu, Y., Südhof, T.C., and Wernig, M. (2021). Efficient generation of dopaminergic induced neuronal cells with midbrain characteristics. Stem Cell Reports *16*, 1763-1776. 10.1016/j.stemcr.2021.05.017.

27. Subach, O.M., Cranfill, P.J., Davidson, M.W., and Verkhusha, V.V. (2011). An enhanced monomeric blue fluorescent protein with the high chemical stability of the chromophore. PLoS One *6*, e28674. 10.1371/journal.pone.0028674.

28. Müller-Kuller, U., Ackermann, M., Kolodziej, S., Brendel, C., Fritsch, J., Lachmann, N., Kunkel, H., Lausen, J., Schambach, A., Moritz, T., and Grez, M. (2015). A minimal ubiquitous chromatin opening element (UCOE) effectively prevents silencing of juxtaposed

1011 heterologous promoters by epigenetic remodeling in multipotent and pluripotent stem
1012 cells. Nucleic Acids Res *43*, 1577-1592. 10.1093/nar/gkv019.

1013 29. Chung, J.H., Bell, A.C., and Felsenfeld, G. (1997). Characterization of the chicken beta-
1014 globin insulator. Proc Natl Acad Sci U S A *94*, 575-580. 10.1073/pnas.94.2.575.

1015 30. Rasmussen, Mikkel A., Holst, B., Tümer, Z., Johnsen, Mads G., Zhou, S., Stummann, Tina C.,
1016 Hyttel, P., and Clausen, C. (2014). Transient p53 Suppression Increases Reprogramming
1017 of Human Fibroblasts without Affecting Apoptosis and DNA Damage. Stem Cell Reports
1018 *3*, 404-413. 10.1016/j.stemcr.2014.07.006.

1019 31. Js, J., R.H., Shaib, A.H., Rehbach, K., Lee, C., Seif, P., Thomas, C., Gideons, E., Guenther, A.,
1020 Krutenko, T., et al. (2019). An Autaptic Culture System for Standardized Analyses of iPSC-
1021 Derived Human Neurons. Cell reports *27*. 10.1016/j.celrep.2019.04.059.

1022 32. Jones, M.V., and Westbrook, G.L. (1995). Desensitized states prolong GABAA channel
1023 responses to brief agonist pulses. Neuron *15*, 181-191. 10.1016/0896-6273(95)90075-
1024 6.

1025 33. M., M., Rehbach, K., Brunner, J.W., Classen, J.A., Lammertse, H.C.A., van Linge, L.A., Schut,
1026 D., Krutenko, T., Hebisch, M., Cornelisse, L.N., et al. (2019). A Single-Cell Model for
1027 Synaptic Transmission and Plasticity in Human iPSC-Derived Neurons. Cell reports *27*.
1028 10.1016/j.celrep.2019.04.058.

1029 34. Pantazis, C.B., Yang, A., Lara, E., McDonough, J.A., Blauwendraat, C., Peng, L., Oguro, H.,
1030 Kanaujiya, J., Zou, J., Sebesta, D., et al. (2022). A reference human induced pluripotent
1031 stem cell line for large-scale collaborative studies. Cell Stem Cell *29*, 1685-1702.e1622.
1032 10.1016/j.stem.2022.11.004.

1033 35. Nadadhur, A.G., Alsaqati, M., Gasparotto, L., Cornelissen-Steijger, P., van Hugte, E., Dooves,
1034 S., Harwood, A.J., and Heine, V.M. (2019). Neuron-Glia Interactions Increase Neuronal
1035 Phenotypes in Tuberous Sclerosis Complex Patient iPSC-Derived Models. Stem Cell
1036 Reports *12*, 42-56. 10.1016/j.stemcr.2018.11.019.

1037 36. Loomba, S., Straehle, J., Gangadharan, V., Heike, N., Khalifa, A., Motta, A., Ju, N., Sievers,
1038 M., Gempt, J., Meyer, H.S., and Helmstaedter, M. (2022). Connectomic comparison of
1039 mouse and human cortex. Science *377*. 10.1126/science.abo0924.

1040 37. Bakken, T.E., Jorstad, N.L., Hu, Q., Lake, B.B., Tian, W., Kalmbach, B.E., Crow, M., Hodge, R.D.,
1041 Krienen, F.M., Sorensen, S.A., et al. (2021). Comparative cellular analysis of motor cortex
1042 in human, marmoset and mouse. Nature *598*, 111-119. 10.1038/s41586-021-03465-8.

1043 38. Fang, R., Xia, C., Close, J.L., Zhang, M., He, J., Huang, Z., Halpern, A.R., Long, B., Miller, J.A.,
1044 Lein, E.S., and Zhuang, X. (2022). Conservation and divergence of cortical cell

organization in human and mouse revealed by MERFISH. Science *377*, 56-62. 10.1126/science.abm1741.

39. Chanda, S., Ang, Cheen E., Davila, J., Pak, C., Mall, M., Lee, Qian Y., Ahlenius, H., Jung, Seung W., Südhof, Thomas C., and Wernig, M. (2014). Generation of Induced Neuronal Cells by the Single Reprogramming Factor ASCL1. Stem Cell Reports *3*, 282-296. 10.1016/j.stemcr.2014.05.020.

40. Jorstad, N.L., Close, J., Johansen, N., Yanny, A.M., Barkan, E.R., Travaglini, K.J., Bertagnolli, D., Campos, J., Casper, T., Crichton, K., et al. (2023). Transcriptomic cytoarchitecture reveals principles of human neocortex organization. Science *382*. 10.1126/science.adf6812.

41. Skene, N.G., and Grant, S.G. (2016). Identification of Vulnerable Cell Types in Major Brain Disorders Using Single Cell Transcriptomes and Expression Weighted Cell Type Enrichment. Front Neurosci *10*, 16. 10.3389/fnins.2016.00016.

42. Dixon, C., Sah, P., Lynch, J.W., and Keramidas, A. (2014). GABA_A Receptor α and γ Subunits Shape Synaptic Currents via Different Mechanisms *. Journal of Biological Chemistry *289*, 5399-5411. 10.1074/jbc.M113.514695.

43. Zhang, S.J., Huguenard, J.R., and Prince, D.A. (1997). GABAA Receptor-Mediated Cl– Currents in Rat Thalamic Reticular and Relay Neurons. Journal of Neurophysiology *78*, 2280-2286. 10.1152/jn.1997.78.5.2280.

44. Koopmans, F., Van Nierop, P., Andres-Alonso, M., Byrnes, A., Cijsouw, T., Coba, M.P., Cornelisse, L.N., Farrell, R.J., Goldschmidt, H.L., Howrigan, D.P., et al. (2019). SynGO: An Evidence-Based, Expert-Curated Knowledge Base for the Synapse. Neuron *103*, 217-234.e214. 10.1016/j.neuron.2019.05.002.

45. Koopmans, F. (2024). GOAT: efficient and robust identification of gene set enrichment. Communications Biology *7*, 744. 10.1038/s42003-024-06454-5.

46. Paraskevopoulou, F., Herman, M.A., and Rosenmund, C. (2019). Glutamatergic Innervation onto Striatal Neurons Potentiates GABAergic Synaptic Output. J Neurosci *39*, 4448-4460. 10.1523/jneurosci.2630-18.2019.

47. Watanabe, M., and Fukuda, A. (2015). Development and regulation of chloride homeostasis in the central nervous system. Front Cell Neurosci *9*, 371. 10.3389/fncel.2015.00371.

48. Roig Adam, A., Martínez-López, J.A., Van Der Spek, S.J.F., Achsel, T., Andres-Alonso, M., Bagni, C., Bayés, À., Biederer, T., Brose, N., Chua, J.J.E., et al. (2023). Transcriptional

diversity in specific synaptic gene sets discriminates cortical neuronal identity. Biology Direct *18*. 10.1186/s13062-023-00372-y.

49. Ikeda, K., Yanagawa, Y., and Bekkers, J.M. (2008). Distinctive Quantal Properties of Neurotransmission at Excitatory and Inhibitory Autapses Revealed Using Variance–Mean Analysis. The Journal of Neuroscience *28*, 13563-13573. 10.1523/jneurosci.3350-08.2008.

50. Jiang, L., Sun, S., Nedergaard, M., and Kang, J. (2000). Paired-pulse modulation at individual GABAergic synapses in rat hippocampus. J Physiol *523 Pt 2*, 425-439. 10.1111/j.1469-7793.2000.t01-1-00425.x.

51. Lambert, N.A., and Wilson, W.A. (1994). Temporally distinct mechanisms of use-dependent depression at inhibitory synapses in the rat hippocampus in vitro. Journal of neurophysiology *72*, 121-130.

52. Pearce, R.A., Grunder, S.D., and Faucher, L.D. (1995). Different mechanisms for use-dependent depression of two GABAA-mediated IPSCs in rat hippocampus. J Physiol *484 (Pt 2)*, 425-435. 10.1113/jphysiol.1995.sp020675.

53. Rebollo, B., Abrahamyan, A., Thomale, U.-W., Kaindl, A.M., Herman, M.A., and Rosenmund, C. (2025). GABAergic synaptic components are largely preserved across human and mouse neuronal models. Frontiers in Cellular Neuroscience *Volume 19 - 2025*. 10.3389/fncel.2025.1588894.

54. Gonzalez-Ramos, A., Waloschková, E., Mikroulis, A., Kokaia, Z., Bengzon, J., Ledri, M., Andersson, M., and Kokaia, M. (2021). Human stem cell-derived GABAergic neurons functionally integrate into human neuronal networks. Sci Rep *11*, 22050. 10.1038/s41598-021-01270-x.

55. Song, S., Ashok, A., Williams, D., Kaufman, M., Duff, K., and Sproul, A. (2021). Efficient Derivation of Excitatory and Inhibitory Neurons from Human Pluripotent Stem Cells Stably Expressing Direct Reprogramming Factors. Curr Protoc *1*, e141. 10.1002/cpz1.141.

56. Barretto, N., Zhang, H., Powell, S.K., Fernando, M.B., Zhang, S., Flaherty, E.K., Ho, S.M., Slesinger, P.A., Duan, J., and Brennand, K.J. (2020). ASCL1- and DLX2-induced GABAergic neurons from hiPSC-derived NPCs. J Neurosci Methods *334*, 108548. 10.1016/j.jneumeth.2019.108548.

57. Marcó de la Cruz, B., Campos, J., Molinaro, A., Xie, X., Jin, G., Wei, Z., Acuna, C., and Sterky, F.H. (2024). Liprin-α proteins are master regulators of human presynapse assembly. Nature Neuroscience *27*, 629-642. 10.1038/s41593-024-01592-9.

1112 58. Sanchez-Priego, C., Hu, R., Boshans, L.L., Lalli, M., Janas, J.A., Williams, S.E., Dong, Z., and
1113 Yang, N. (2022). Mapping cis-regulatory elements in human neurons links psychiatric
1114 disease heritability and activity-regulated transcriptional programs. Cell Reports *39*,
1115 110877. https://doi.org/10.1016/j.celrep.2022.110877.

1116 59. Clifford, M.A., Athar, W., Leonard, C.E., Russo, A., Sampognaro, P.J., Van der Goes, M.S.,
1117 Burton, D.A., Zhao, X., Lalchandani, R.R., Sahin, M., et al. (2014). EphA7 signaling guides
1118 cortical dendritic development and spine maturation. Proc Natl Acad Sci U S A *111*, 4994-
1119 4999. 10.1073/pnas.1323793111.

1120 60. Wu, J., Ren, J., Cui, H., Xie, Y., and Tang, Y. (2024). Rapid and high-purity differentiation of
1121 human medium spiny neurons reveals LMNB1 hypofunction and subtype necessity in
1122 modeling Huntington's disease. Inflamm Regen *44*, 7. 10.1186/s41232-024-00320-x.

1123 61. Gierman, H.J., Indemans, M.H., Koster, J., Goetze, S., Seppen, J., Geerts, D., van Driel, R.,
1124 and Versteeg, R. (2007). Domain-wide regulation of gene expression in the human
1125 genome. Genome Res *17*, 1286-1295. 10.1101/gr.6276007.

1126 62. Liew, C.-G., Draper, J.S., Walsh, J., Moore, H., and Andrews, P.W. (2007). Transient and Stable
1127 Transgene Expression in Human Embryonic Stem Cells. Stem Cells *25*, 1521-1528.
1128 10.1634/stemcells.2006-0634.

1129 63. Kwak, C.S., Oflaz, F.E., Qiu, J., and Wang, X. (2024). Human stem cell-specific epigenetic
1130 signatures control transgene expression. Biochimica et Biophysica Acta (BBA) - Gene
1131 Regulatory Mechanisms *1867*, 195063. https://doi.org/10.1016/j.bbagrm.2024.195063.

1132 64. He, J., Yang, Q., and Chang, L.-J. (2005). Dynamic DNA Methylation and Histone
1133 Modifications Contribute to Lentiviral Transgene Silencing in Murine Embryonic
1134 Carcinoma Cells. Journal of Virology *79*, 13497-13508. doi:10.1128/jvi.79.21.13497-
1135 13508.2005.

1136 65. Gödecke, N., Zha, L., Spencer, S., Behme, S., Riemer, P., Rehli, M., Hauser, H., and Wirth, D.
1137 (2017). Controlled re-activation of epigenetically silenced Tet promoter-driven
1138 transgene expression by targeted demethylation. Nucleic Acids Research *45*, e147-e147.
1139 10.1093/nar/gkx601.

1140 66. Allison, T., Langerman, J., Sabri, S., Otero-Garcia, M., Lund, A., Huang, J., Wei, X.,
1141 Samarasinghe, R.A., Polioudakis, D., Mody, I., et al. (2021). Defining the nature of human
1142 pluripotent stem cell-derived interneurons via single-cell analysis. Stem Cell Reports
1143 *16*, 2548-2564. https://doi.org/10.1016/j.stemcr.2021.08.006.

1144 67. Lindhout, F.W., Kooistra, R., Portegies, S., Herstel, L.J., Stucchi, R., Snoek, B.L., Altelaar,
1145 A.F.M., MacGillavry, H.D., Wierenga, C.J., and Hoogenraad, C.C. (2020). Quantitative

mapping of transcriptome and proteome dynamics during polarization of human iPSC-derived neurons. eLife *9*, e58124. 10.7554/eLife.58124.

68. Titlow, J.S., Kiourlappou, M., Palanca, A., Lee, J.Y., Gala, D.S., Ennis, D., Yu, J.J.S., Young, F.L., Susano Pinto, D.M., Garforth, S., et al. (2023). Systematic analysis of YFP traps reveals common mRNA/protein discordance in neural tissues. Journal of Cell Biology *222*, e202205129. 10.1083/jcb.202205129.

69. Moritz, C.P., Mühlhaus, T., Tenzer, S., Schulenborg, T., and Friauf, E. (2019). Poor transcript-protein correlation in the brain: negatively correlating gene products reveal neuronal polarity as a potential cause. Journal of Neurochemistry *149*, 582-604. https://doi.org/10.1111/jnc.14664.

70. Lin, H.-C., Janssens, J., Eisinger, B., Hornauer, P., Kroell, A.-S., Santel, M., Pascual-Garcia, M., Okamoto, R., Karava, K., He, Z., et al. (2025). Human neuron subtype programming via single-cell transcriptome-coupled patterning screens. Science *389*, eadn6121. doi:10.1126/science.adn6121.

71. Müller, M., Felmy, F., Schwaller, B., and Schneggenburger, R. (2007). Parvalbumin is a mobile presynaptic Ca2+ buffer in the calyx of Held that accelerates the decay of Ca2+ and short-term facilitation. J Neurosci *27*, 2261-2271. 10.1523/jneurosci.5582-06.2007.

72. Pór, A., Pocsai, K., Rusznák, Z., and Szucs, G. (2005). Presence and distribution of three calcium binding proteins in projection neurons of the adult rat cochlear nucleus. Brain Res *1039*, 63-74. 10.1016/j.brainres.2005.01.057.

73. Laing, B.T., Anderson, M.S., Bonaventura, J., Jayan, A., Sarsfield, S., Gajendiran, A., Michaelides, M., and Aponte, Y. (2023). Anterior hypothalamic parvalbumin neurons are glutamatergic and promote escape behavior. Curr Biol *33*, 3215-3228.e3217. 10.1016/j.cub.2023.06.070.

74. Gartner, W., Lang, W., Leutmetzer, F., Domanovits, H., Waldhäusl, W., and Wagner, L. (2001). Cerebral Expression and Serum Detectability of Secretagogin, a Recently Cloned EF-hand Ca2+ -binding Protein. Cerebral Cortex *11*, 1161-1169. 10.1093/cercor/11.12.1161.

75. Tu, Y., Qin, J., Zhang, Q.M., Tang, T.S., Wang, L., and Yao, J. (2023). Secretagogin regulates asynchronous and spontaneous glutamate release in hippocampal neurons through interaction with Doc2 α . Life Med *2*, lnad041. 10.1093/lifemedi/lnad041.

76. Hanics, J., Tretiakov, E.O., Romanov, R.A., Gáspárdy, A., Hevesi, Z., Schnell, R., Harkany, T., and Alpár, A. (2025). Neuronal activity modulates the expression of secretagogin, a Ca(2+) sensor protein, during mammalian forebrain development. Acta Physiol (Oxf) *241*, e70031. 10.1111/apha.70031.

1180 77. Lin, H.-C., He, Z., Ebert, S., Schörnig, M., Santel, M., Nikolova, M.T., Weigert, A., Hevers, W.,
1181 Kasri, N.N., Taverna, E., et al. (2021). NGN2 induces diverse neuron types from human
1182 pluripotency. Stem cell reports *16*, 2118-2127. 10.1016/j.stemcr.2021.07.006.

1183 78. Nehme, R., Zuccaro, E., Ghosh, S.D., Li, C., Sherwood, J.L., Pietilainen, O., Barrett, L.E.,
1184 Limone, F., Worringer, K.A., Kommineni, S., et al. (2018). Combining NGN2 Programming
1185 with Developmental Patterning Generates Human Excitatory Neurons with NMDAR-
1186 Mediated Synaptic Transmission. Cell Reports *23*, 2509-2523.
1187 10.1016/j.celrep.2018.04.066.

1188 79. Rhee, H.J., Shaib, A.H., Rehbach, K., Lee, C., Seif, P., Thomas, C., Gideons, E., Guenther, A.,
1189 Krutenko, T., Hebisch, M., et al. (2019). An Autaptic Culture System for Standardized
1190 Analyses of iPSC-Derived Human Neurons. Cell Reports *27*, 2212-2228.e2217.
1191 https://doi.org/10.1016/j.celrep.2019.04.059.

1192 80. Bullmann, T., Kaas, T., Ritzau-Jost, A., Wöhner, A., Kirmann, T., Rizalar, F.S., Holzer, M.,
1193 Nerlich, J., Puchkov, D., Geis, C., et al. (2024). Human iPSC-Derived Neurons with Reliable
1194 Synapses and Large Presynaptic Action Potentials. J Neurosci *44*.
1195 10.1523/jneurosci.0971-23.2024.

1196 81. van Berkel, A.A., Lammertse, H.C.A., Öttl, M., Koopmans, F., Misra-Isrie, M., Meijer, M.,
1197 Dilena, R., van Hasselt, P.M., Engelen, M., van Haelst, M., et al. (2024). Reduced MUNC18-
1198 1 Levels, Synaptic Proteome Changes, and Altered Network Activity in STXBP1-Related
1199 Disorder Patient Neurons. Biol Psychiatry Glob Open Sci *4*, 284-298.
1200 10.1016/j.bpsgos.2023.05.004.

1201 82. Fenske, P., Grauel, M.K., Brockmann, M.M., Dorrn, A.L., Trimbuch, T., and Rosenmund, C.
1202 (2019). Autaptic cultures of human induced neurons as a versatile platform for studying
1203 synaptic function and neuronal morphology. Scientific Reports *9*, 4890. 10.1038/s41598-
1204 019-41259-1.

1205 83. Togo, K., Fukusumi, H., Shofuda, T., Ohnishi, H., Yamazaki, H., Hayashi, M.K., Kawasaki, N.,
1206 Takei, N., Nakazawa, T., Saito, Y., et al. (2021). Postsynaptic structure formation of human
1207 iPS cell-derived neurons takes longer than presynaptic formation during neural
1208 differentiation in vitro. Molecular Brain *14*, 149. 10.1186/s13041-021-00851-1.

1209 84. Nadadhur, A.G., Emperador Melero, J., Meijer, M., Schut, D., Jacobs, G., Li, K.W., Hjorth, J.J.J.,
1210 Meredith, R.M., Toonen, R.F., Van Kesteren, R.E., et al. (2017). Multi-level characterization
1211 of balanced inhibitory-excitatory cortical neuron network derived from human
1212 pluripotent stem cells. PLOS ONE *12*, e0178533. 10.1371/journal.pone.0178533.

1213 85. Friedman, H.V., Bresler, T., Garner, C.C., and Ziv, N.E. (2000). Assembly of New Individual
1214 Excitatory Synapses: Time Course and Temporal Order of Synaptic Molecule
1215 Recruitment. Neuron *27*, 57-69. 10.1016/S0896-6273(00)00009-X.

1216 86. Kwon, H.B., and Sabatini, B.L. (2011). Glutamate induces de novo growth of functional
1217 spines in developing cortex. Nature *474*, 100-104. 10.1038/nature09986.

1218 87. Richards, D.A., Mateos, J.M., Hugel, S., de Paola, V., Caroni, P., Gähwiler, B.H., and McKinney,
1219 R.A. (2005). Glutamate induces the rapid formation of spine head protrusions in
1220 hippocampal slice cultures. Proc Natl Acad Sci U S A *102*, 6166-6171.
1221 10.1073/pnas.0501881102.

1222 88. Mammen, A.L., Huganir, R.L., and O'Brien, R.J. (1997). Redistribution and Stabilization of
1223 Cell Surface Glutamate Receptors during Synapse Formation. The Journal of
1224 Neuroscience *17*, 7351-7358. 10.1523/jneurosci.17-19-07351.1997.

1225 89. Petralia, R.S. (2012). Distribution of Extrasynaptic NMDA Receptors on Neurons. The
1226 Scientific World Journal *2012*, 267120. https://doi.org/10.1100/2012/267120.

1227 90. Okabe, S., Miwa, A., and Okado, H. (2001). Spine formation and correlated assembly of
1228 presynaptic and postsynaptic molecules. J Neurosci *21*, 6105-6114.
1229 10.1523/jneurosci.21-16-06105.2001.

1230 91. Andreae, L.C., and Burrone, J. (2015). Spontaneous Neurotransmitter Release Shapes
1231 Dendritic Arbors via Long-Range Activation of NMDA Receptors. Cell Rep *10*, 873-882.
1232 10.1016/j.celrep.2015.01.032.

1233 92. Sanes, J.R., and Lichtman, J.W. (1999). Development of the vertebrate neuromuscular
1234 junction. Annu Rev Neurosci *22*, 389-442. 10.1146/annurev.neuro.22.1.389.

1235 93. Harms, K.J., Tovar, K.R., and Craig, A.M. (2005). Synapse-specific regulation of AMPA
1236 receptor subunit composition by activity. J Neurosci *25*, 6379-6388.
1237 10.1523/jneurosci.0302-05.2005.

1238 94. MacGillavry, H.D., Song, Y., Raghavachari, S., and Blanpied, T.A. (2013). Nanoscale
1239 scaffolding domains within the postsynaptic density concentrate synaptic AMPA
1240 receptors. Neuron *78*, 615-622. 10.1016/j.neuron.2013.03.009.

1241 95. Vaughan, P.F., Walker, J.H., and Peers, C. (1998). The regulation of neurotransmitter
1242 secretion by protein kinase C. Mol Neurobiol *18*, 125-155. 10.1007/bf02914269.

1243 96. Cui, Y., Costa, R.M., Murphy, G.G., Elgersma, Y., Zhu, Y., Gutmann, D.H., Parada, L.F., Mody,
1244 I., and Silva, A.J. (2008). Neurofibromin regulation of ERK signaling modulates GABA
1245 release and learning. Cell *135*, 549-560. 10.1016/j.cell.2008.09.060.

97. Lützenkirchen, F.P., Zhu, Y., Maric, H.M., Boeck, D.S., Gromova, K.V., and Kneussel, M. (2024). Neurobeachin regulates receptor downscaling at GABAergic inhibitory synapses in a protein kinase A-dependent manner. Communications Biology *7*, 1635. 10.1038/s42003-024-07294-z.

98. Ghosh, H., Auguadri, L., Battaglia, S., Simone Thirouin, Z., Zemoura, K., Messner, S., Acuña, M.A., Wildner, H., Yévenes, G.E., Dieter, A., et al. (2016). Several posttranslational modifications act in concert to regulate gephyrin scaffolding and GABAergic transmission. Nature Communications *7*, 13365. 10.1038/ncomms13365.

99. Tyagarajan, S.K., Ghosh, H., Yévenes, G.E., Imanishi, S.Y., Zeilhofer, H.U., Gerrits, B., and Fritschy, J.M. (2013). Extracellular signal-regulated kinase and glycogen synthase kinase 3 β regulate gephyrin postsynaptic aggregation and GABAergic synaptic function in a calpain-dependent mechanism. J Biol Chem *288*, 9634-9647. 10.1074/jbc.M112.442616.

100. Tyagarajan, S.K., Ghosh, H., Yévenes, G.E., Nikonenko, I., Ebeling, C., Schwerdel, C., Sidler, C., Zeilhofer, H.U., Gerrits, B., Muller, D., and Fritschy, J.M. (2011). Regulation of GABAergic synapse formation and plasticity by GSK3beta-dependent phosphorylation of gephyrin. Proc Natl Acad Sci U S A *108*, 379-384. 10.1073/pnas.1011824108.

101. Bright, D.P., and Smart, T.G. (2013). Protein kinase C regulates tonic GABAA receptor-mediated inhibition in the hippocampus and thalamus. European Journal of Neuroscience *38*, 3408-3423. https://doi.org/10.1111/ejn.12352.

102. Lützenkirchen, F.P., Zhu, Y., Maric, H.M., Boeck, D.S., Gromova, K.V., and Kneussel, M. (2024). Neurobeachin regulates receptor downscaling at GABAergic inhibitory synapses in a protein kinase A-dependent manner. Commun Biol *7*, 1635. 10.1038/s42003-024-07294-z.

103. Farzana, F., Zalm, R., Chen, N., Li, K.W., Grant, S.G., Smit, A.B., Toonen, R.F., and Verhage, M. (2016). Neurobeachin Regulates Glutamate- and GABA-Receptor Targeting to Synapses via Distinct Pathways. Mol Neurobiol *53*, 2112-2123. 10.1007/s12035-015-9164-8.

104. Hausrat, T.J., Muhia, M., Gerrow, K., Thomas, P., Hirdes, W., Tsukita, S., Heisler, F.F., Herich, L., Dubroqua, S., Breiden, P., et al. (2015). Radixin regulates synaptic GABAA receptor density and is essential for reversal learning and short-term memory. Nat Commun *6*, 6872. 10.1038/ncomms7872.

105. Nakamura, Y., Darnieder, L.M., Deeb, T.Z., and Moss, S.J. (2015). Regulation of GABAARs by phosphorylation. Adv Pharmacol *72*, 97-146. 10.1016/bs.apha.2014.11.008.

1279 106. Song, S.-H., and Augustine, G.J. (2023). Different mechanisms of synapsin-induced vesicle
1280 clustering at inhibitory and excitatory synapses. Cell Reports *42*.
1281 10.1016/j.celrep.2023.113004.

1282 107. Flores, C.E., Nikonenko, I., Mendez, P., Fritschy, J.M., Tyagarajan, S.K., and Muller, D. (2015).
1283 Activity-dependent inhibitory synapse remodeling through gephyrin phosphorylation.
1284 Proc Natl Acad Sci U S A *112*, E65-72. 10.1073/pnas.1411170112.

1285 108. Hao, Y., Liu, H., Zeng, X.-T., Wang, Y., Zeng, W.-X., Qian, K.-Y., Li, L., Chi, M.-X., Gao, S., Hu, Z.,
1286 and Tong, X.-J. (2023). UNC-43/CaMKII-triggered anterograde signals recruit GABAARs to
1287 mediate inhibitory synaptic transmission and plasticity at C. elegans NMJs. Nature
1288 Communications *14*, 1436. 10.1038/s41467-023-37137-0.

1289 109. Houston, C.M., He, Q., and Smart, T.G. (2009). CaMKII phosphorylation of the GABA(A)
1290 receptor: receptor subtype- and synapse-specific modulation. J Physiol *587*, 2115-2125.
1291 10.1113/jphysiol.2009.171603.

1292 110. Lorenz-Guertin, J.M., and Jacob, T.C. (2018). GABA type a receptor trafficking and the
1293 architecture of synaptic inhibition. Developmental Neurobiology *78*, 238-270.
1294 https://doi.org/10.1002/dneu.22536.

1295 111. Heisler, F.F., Loebrich, S., Pechmann, Y., Maier, N., Zivkovic, A.R., Tokito, M., Hausrat, T.J.,
1296 Schweizer, M., Bähring, R., Holzbaur, E.L., et al. (2011). Muskelin regulates actin filament-
1297 and microtubule-based GABA(A) receptor transport in neurons. Neuron *70*, 66-81.
1298 10.1016/j.neuron.2011.03.008.

1299 112. Velasco, C.D., Santarella-Mellwig, R., Schorb, M., Gao, L., Thorn-Seshold, O., and Llobet,
1300 A. (2023). Microtubule depolymerization contributes to spontaneous neurotransmitter
1301 release in vitro. Communications Biology *6*, 488. 10.1038/s42003-023-04779-1.

1302 113. Waites, C., Qu, X., and Bartolini, F. (2021). The synaptic life of microtubules. Curr Opin
1303 Neurobiol *69*, 113-123. 10.1016/j.conb.2021.03.004.

1304 114. Jacob, T.C., Moss, S.J., and Jurd, R. (2008). GABA(A) receptor trafficking and its role in the
1305 dynamic modulation of neuronal inhibition. Nat Rev Neurosci *9*, 331-343.
1306 10.1038/nrn2370.

1307 115. Prag, S., De Arcangelis, A., Georges-Labouesse, E., and Adams, J.C. (2007). Regulation of
1308 post-translational modifications of muskelin by protein kinase C. The International
1309 Journal of Biochemistry & Cell Biology *39*, 366-378.
1310 https://doi.org/10.1016/j.biocel.2006.09.003.

1311 116. Biederer, T., Kaeser, P.S., and Blanpied, T.A. (2017). Transcellular Nanoalignment of
1312 Synaptic Function. Neuron *96*, 680-696. 10.1016/j.neuron.2017.10.006.

1313 117. Tang, A.H., Chen, H., Li, T.P., Metzbower, S.R., MacGillavry, H.D., and Blanpied, T.A. (2016).
1314 A trans-synaptic nanocolumn aligns neurotransmitter release to receptors. Nature *536*,
1315 210-214. 10.1038/nature19058.

1316 118. Scimemi, A., and Diamond, J.S. (2012). The number and organization of Ca2+ channels in
1317 the active zone shapes neurotransmitter release from Schaffer collateral synapses. J
1318 Neurosci *32*, 18157-18176. 10.1523/jneurosci.3827-12.2012.

1319 119. Sanderson, T.M., Georgiou, J., and Collingridge, G.L. (2020). Illuminating Relationships
1320 Between the Pre- and Post-synapse. Front Neural Circuits *14*, 9.
1321 10.3389/fncir.2020.00009.

1322 120. Südhof, T.C. (2021). The cell biology of synapse formation. J Cell Biol *220*.
1323 10.1083/jcb.202103052.

1324 121. Südhof, T.C. (2018). Towards an Understanding of Synapse Formation. Neuron *100*, 276-
1325 293. 10.1016/j.neuron.2018.09.040.

1326 122. Olah, S.S., Kareemo, D.J., Buchta, W.C., Sinnen, B.L., Miller, C.N., Actor-Engel, H.S., Gookin,
1327 S.E., Winborn, C.S., Kleinjan, M.S., Crosby, K.C., et al. (2023). Acute reorganization of
1328 postsynaptic GABA_A receptors reveals the functional impact of molecular
1329 nanoarchitecture at inhibitory synapses. Cell Reports *42*. 10.1016/j.celrep.2023.113331.

1330 123. Karayannis, T., Au, E., Patel, J.C., Kruglikov, I., Markx, S., Delorme, R., Héron, D., Salomon,
1331 D., Glessner, J., Restituito, S., et al. (2014). Cntnap4 differentially contributes to GABAergic
1332 and dopaminergic synaptic transmission. Nature *511*, 236-240. 10.1038/nature13248.

1333 124. Um, J.W., Kim, K.H., Park, B.S., Choi, Y., Kim, D., Kim, C.Y., Kim, S.J., Kim, M., Ko, J.S., Lee, S.-
1334 G., et al. (2014). Structural basis for LAR-RPTP/Slitrk complex-mediated synaptic
1335 adhesion. Nature Communications *5*, 5423. 10.1038/ncomms6423.

1336 125. Fiederling, A., Ewert, R., Andreyeva, A., Jüngling, K., and Gottmann, K. (2011). E-cadherin
1337 is required at GABAergic synapses in cultured cortical neurons. Neuroscience Letters
1338 *501*, 167-172. https://doi.org/10.1016/j.neulet.2011.07.009.

1339 126. Beuter, S., Ardi, Z., Horovitz, O., Wuchter, J., Keller, S., Saha, R., Tripathi, K., Anunu, R., Kehat,
1340 O., Kriebel, M., et al. (2016). Receptor tyrosine kinase EphA7 is required for interneuron
1341 connectivity at specific subcellular compartments of granule cells. Scientific Reports *6*,
1342 29710. 10.1038/srep29710.

1343 127. Park, Y.K., and Goda, Y. (2016). Integrins in synapse regulation. Nature Reviews
1344 Neuroscience *17*, 745-756. 10.1038/nrn.2016.138.

128. Sia, G.-M., Béïque, J.-C., Rumbaugh, G., Cho, R., Worley, P.F., and Huganir, R.L. (2007). Interaction of the N-Terminal Domain of the AMPA Receptor GluR4 Subunit with the Neuronal Pentraxin NP1 Mediates GluR4 Synaptic Recruitment. Neuron *55*, 87-102. 10.1016/j.neuron.2007.06.020.

129. Ray, A., and Treloar, H.B. (2012). IgSF8: a developmentally and functionally regulated cell adhesion molecule in olfactory sensory neuron axons and synapses. Mol Cell Neurosci *50*, 238-249. 10.1016/j.mcn.2012.05.007.

130. Li, W., Yang, L., Tang, C., Liu, K., Lu, Y., Wang, H., Yan, K., Qiu, Z., and Zhou, W. (2020). Mutations of CNTNAP1 led to defects in neuronal development. JCI Insight *5*. 10.1172/jci.insight.135697.

131. Wiera, G., Brzdąk, P., Lech, A.M., Lebida, K., Jabłońska, J., Gmerek, P., and Mozrzymas, J.W. (2022). Integrins Bidirectionally Regulate the Efficacy of Inhibitory Synaptic Transmission and Control GABAergic Plasticity. J Neurosci *42*, 5830-5842. 10.1523/jneurosci.1458-21.2022.

132. Tucić, M., Stamenković, V., and Andjus, P. (2021). The Extracellular Matrix Glycoprotein Tenascin C and Adult Neurogenesis. Front Cell Dev Biol *9*, 674199. 10.3389/fcell.2021.674199.

133. Quattrocchi, C.C., Wannenes, F., Persico, A.M., Ciafré, S.A., D'Arcangelo, G., Farace, M.G., and Keller, F. (2002). Reelin is a serine protease of the extracellular matrix. J Biol Chem *277*, 303-309. 10.1074/jbc.M106996200.

134. O'Brien, R.J., Xu, D., Petralia, R.S., Steward, O., Huganir, R.L., and Worley, P. (1999). Synaptic clustering of AMPA receptors by the extracellular immediate-early gene product Narp. Neuron *23*, 309-323. 10.1016/s0896-6273(00)80782-5.

135. Yim, Y.S., Kwon, Y., Nam, J., Yoon, H.I., Lee, K., Kim, D.G., Kim, E., Kim, C.H., and Ko, J. (2013). Slitrks control excitatory and inhibitory synapse formation with LAR receptor protein tyrosine phosphatases. Proc Natl Acad Sci U S A *110*, 4057-4062. 10.1073/pnas.1209881110.

136. Martin, E.E., Wleklinski, E., Hoang, H.T.M., and Ahmad, M. (2021). Interaction and Subcellular Association of PRRT1/SynDIG4 With AMPA Receptors. Frontiers in Synaptic Neuroscience *Volume 13 - 2021*. 10.3389/fnsyn.2021.705664.

137. Matsunaga, H., and Aruga, J. (2021). Trans-Synaptic Regulation of Metabotropic Glutamate Receptors by Elfn Proteins in Health and Disease. Frontiers in Neural Circuits *Volume 15 - 2021*. 10.3389/fncir.2021.634875.

138. Hijazi, S., Heistek, T.S., van der Loo, R., Mansvelder, H.D., Smit, A.B., and van Kesteren, R.E. (2020). Hyperexcitable Parvalbumin Interneurons Render Hippocampal Circuitry Vulnerable to Amyloid Beta. iScience *23*, 101271. 10.1016/j.isci.2020.101271.

139. Mossner, J.M., Batista-Brito, R., Pant, R., and Cardin, J.A. (2020). Developmental loss of MeCP2 from VIP interneurons impairs cortical function and behavior. eLife *9*, e55639. 10.7554/eLife.55639.

140. Malwade, S., Gasthaus, J., Bellardita, C., Andelic, M., Moric, B., Korshunova, I., Kiehn, O., Vasistha, N.A., and Khodosevich, K. (2022). Identification of Vulnerable Interneuron Subtypes in 15q13.3 Microdeletion Syndrome Using Single-Cell Transcriptomics. Biol Psychiatry *91*, 727-739. 10.1016/j.biopsych.2021.09.012.

141. Goel, A., Cantu, D.A., Guilfoyle, J., Chaudhari, G.R., Newadkar, A., Todisco, B., de Alba, D., Kourdougli, N., Schmitt, L.M., Pedapati, E., et al. (2018). Impaired perceptual learning in a mouse model of Fragile X syndrome is mediated by parvalbumin neuron dysfunction and is reversible. Nat Neurosci *21*, 1404-1411. 10.1038/s41593-018-0231-0.

142. Gabitto, M.I., Travaglini, K.J., Rachleff, V.M., Kaplan, E.S., Long, B., Ariza, J., Ding, Y., Mahoney, J.T., Dee, N., Goldy, J., et al. (2023). Integrated multimodal cell atlas of Alzheimer's disease. Res Sq. 10.21203/rs.3.rs-2921860/v1.

143. Zott, B., Busche, M.A., Sperling, R.A., and Konnerth, A. (2018). What Happens with the Circuit in Alzheimer's Disease in Mice and Humans? Annu Rev Neurosci *41*, 277-297. 10.1146/annurev-neuro-080317-061725.

144. van Boven, M.A., Mestroni, M., Zwijnenburg, P.J.G., Verhage, M., and Cornelisse, L.N. (2024). A de novo missense mutation in synaptotagmin-1 associated with neurodevelopmental disorder desynchronizes neurotransmitter release. Mol Psychiatry *29*, 1798-1809. 10.1038/s41380-024-02444-5.

145. Østergaard, M., Barbagallo, P., Frederiksen, H.R.S., Chung, W.K., Møller, R.S., Larsen, M.R., Freude, K., Verhage, M., and Sørensen, J.B. (2025). SNAP25 variant I67N: synaptic phenotypes, drug response and proteome changes in human neurons. Brain. 10.1093/brain/awaf119.

146. Öttl, M., Toonen, R.F., and Verhage, M. (2024). Reduced synaptic depression in human neurons carrying homozygous disease-causing STXBP1 variant L446F. Hum Mol Genet *33*, 991-1000. 10.1093/hmg/ddae035.

147. Schmitz, S.K., Hjorth, J.J., Joemai, R.M., Wijntjes, R., Eijgenraam, S., de Bruijn, P., Georgiou, C., de Jong, A.P., van Ooyen, A., and Verhage, M. (2011). Automated analysis of neuronal

morphology, synapse number and synaptic recruitment. Journal of neuroscience methods *195*, 185-193.

148. Thanou, E., Koopmans, F., Pita-Illobre, D., Klaassen, R.V., Özer, B., Charalampopoulos, I., Smit, A.B., and Li, K.W. (2023). Suspension TRAPping Filter (sTRAP) Sample Preparation for Quantitative Proteomics in the Low µg Input Range Using a Plasmid DNA Micro-Spin Column: Analysis of the Hippocampus from the 5xFAD Alzheimer's Disease Mouse Model. Cells *12*. 10.3390/cells12091242.

149. Demichev, V., Messner, C.B., Vernardis, S.I., Lilley, K.S., and Ralser, M. (2020). DIA-NN: neural networks and interference correction enable deep proteome coverage in high throughput. Nature Methods *17*, 41-44. 10.1038/s41592-019-0638-x.

150. Koopmans, F., Li, K.W., Klaassen, R.V., and Smit, A.B. (2023). MS-DAP Platform for Downstream Data Analysis of Label-Free Proteomics Uncovers Optimal Workflows in Benchmark Data Sets and Increased Sensitivity in Analysis of Alzheimer's Biomarker Data. J Proteome Res *22*, 374-386. 10.1021/acs.jproteome.2c00513.

151. Zhu, Y., Orre, L.M., Zhou Tran, Y., Mermelekas, G., Johansson, H.J., Malyutina, A., Anders, S., and Lehtiö, J. (2020). DEqMS: A Method for Accurate Variance Estimation in Differential Protein Expression Analysis. Mol Cell Proteomics *19*, 1047-1057. 10.1074/mcp.TIR119.001646.

152. Koopmans, F. (2024). GOAT: efficient and robust identification of gene set enrichment. Commun Biol *7*, 744. 10.1038/s42003-024-06454-5.

153. Koopmans, F., van Nierop, P., Andres-Alonso, M., Byrnes, A., Cijsouw, T., Coba, M.P., Cornelisse, L.N., Farrell, R.J., Goldschmidt, H.L., Howrigan, D.P., et al. (2019). SynGO: An Evidence-Based, Expert-Curated Knowledge Base for the Synapse. Neuron *103*, 217-234.e214. 10.1016/j.neuron.2019.05.002.

154. Demichev, V., Szyrwiel, L., Yu, F., Teo, G.C., Rosenberger, G., Niewienda, A., Ludwig, D., Decker, J., Kaspar-Schoenefeld, S., Lilley, K.S., et al. (2022). dia-PASEF data analysis using FragPipe and DIA-NN for deep proteomics of low sample amounts. Nat Commun *13*, 3944. 10.1038/s41467-022-31492-0.

155. Demichev, V., Messner, C.B., Vernardis, S.I., Lilley, K.S., and Ralser, M. (2020). DIA-NN: neural networks and interference correction enable deep proteome coverage in high throughput. Nat Methods *17*, 41-44. 10.1038/s41592-019-0638-x.

156. Huson, V., and Cornelisse, L.N. (2019). viewEPSC.

157. Neher, E. (2015). Merits and limitations of vesicle pool models in view of heterogeneous populations of synaptic vesicles. Neuron *87*, 1131-1142.

158. Wiśniewski, J.R., and Gaugaz, F.Z. (2015). Fast and sensitive total protein and Peptide assays for proteomic analysis. Anal Chem *87*, 4110-4116. 10.1021/ac504689z.

159. Skowronek, P., Thielert, M., Voytik, E., Tanzer, M.C., Hansen, F.M., Willems, S., Karayel, O., Brunner, A.D., Meier, F., and Mann, M. (2022). Rapid and In-Depth Coverage of the (Phospho-)Proteome With Deep Libraries and Optimal Window Design for dia-PASEF. Mol Cell Proteomics *21*, 100279. 10.1016/j.mcpro.2022.100279.

160. Miedema, S.S.M., Mol, M.O., Koopmans, F.T.W., Hondius, D.C., van Nierop, P., Menden, K., de Veij Mestdagh, C.F., van Rooij, J., Ganz, A.B., Paliukhovich, I., et al. (2022). Distinct cell type-specific protein signatures in GRN and MAPT genetic subtypes of frontotemporal dementia. Acta Neuropathologica Communications *10*, 100. 10.1186/s40478-022-01387-8.

161. Team, R. (2020). RStudio: Integrated Development for R (PBC, Boston, MA).

162. Wickham, H. (2016). ggplot2: Elegant Graphics for Data Analysis (Springer International Publishing).

163. Perez-Riverol, Y., Bandla, C., Kundu, D.J., Kamatchinathan, S., Bai, J., Hewapathirana, S., John, N.S., Prakash, A., Walzer, M., Wang, S., and Vizcaíno, J.A. (2025). The PRIDE database at 20 years: 2025 update. Nucleic Acids Res *53*, D543-d553. 10.1093/nar/gkae1011.

Figures

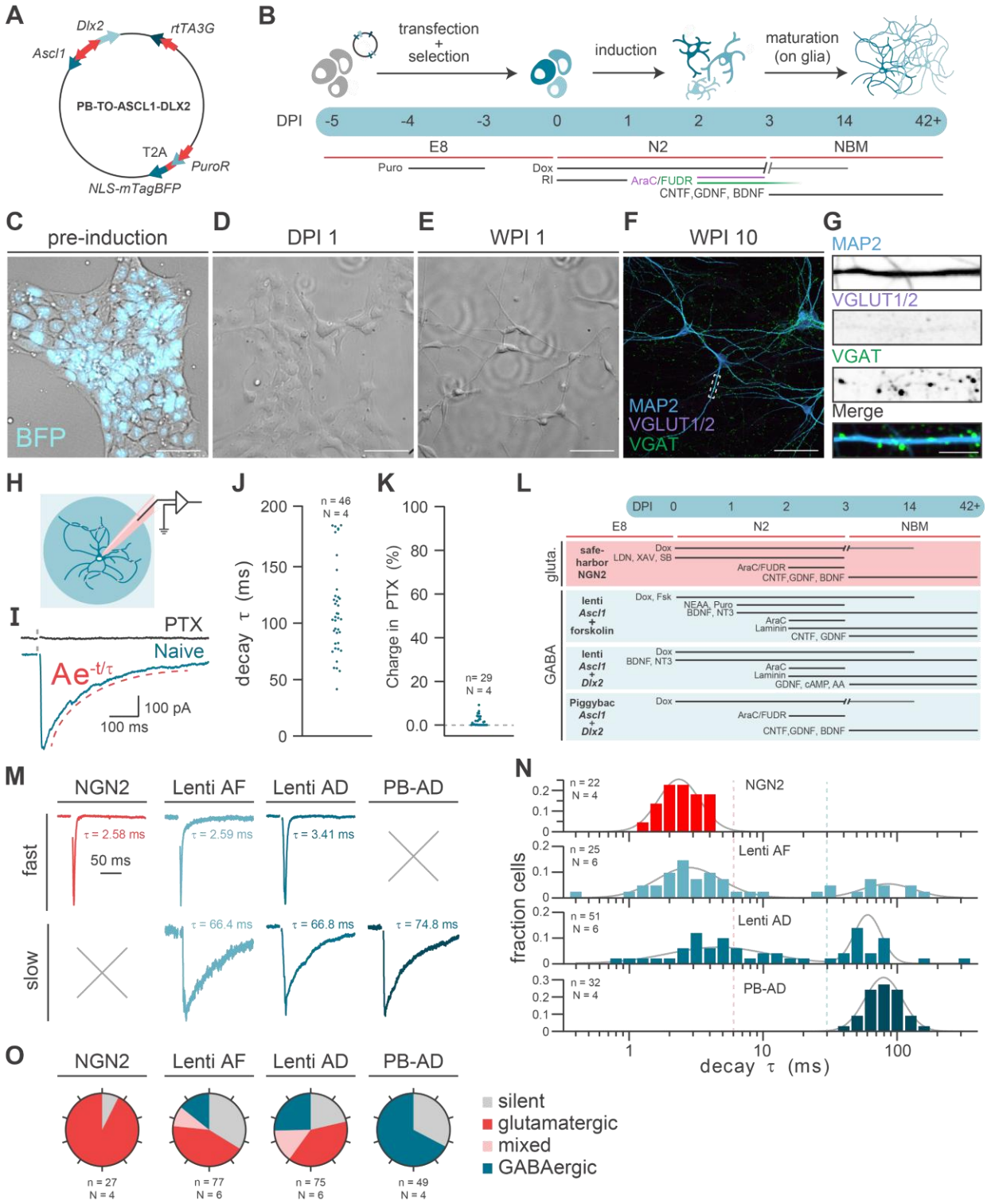

Figure 1. PiggyBac Asc1/Dlx2 efficiently generates pure GABAergic neurons,

A Map of the all-in-one PiggyBac (PB) vector, expressing murine *Ascl1* and *Dlx2* from a bi-directional TRE-responsive promoter, rtTA from the CAG promoter and *pac*-T2A-NLS-mTagBFP from the EF1α promoter. **B** Overview of the protocol for *Ascl1/Dlx2* induction. **C**

Before induction, all iPSCs show nuclear BFP signals, demonstrating successful integration of the PB construct **D** Dox-induced expression of *Dlx2* and *Ascl1* triggers neuronal morphology to arise within one day (DPI1) **E** A week after induction (WPI 1), neural morphology is clearly visible **F** After 10 weeks of culture, PB *Ascl1/Dlx2* induced neurons show mature neuronal morphology with GABAergic synapses (VGAT+ puncta) and no glutamatergic synapses (VGLUT+ puncta) Scale bar: 100 µm **G.** Zoom-in on the dendrite highlighted in F. scale bar = 1 µm. **H** Autaptic cultures of PB *Ascl1/Dlx2* induced neurons were assessed using patch clamp electrophysiology. **I** Evoked postsynaptic currents (PSCs) were fitted using a mono-exponential decay function (red) and their currents were diminished by the application of PTX. **J** Dot-plot of the decay time constants of ePSCs recorded in PB *Ascl1/Dlx2* induced neurons. **K** Dot-plot showing the distribution of cells with 0-10% of the naïve charge remaining in PTX **L** Overview of the four induction methods used, PB *Ascl1/Dlx2* induction was compared to the lentiviral *Ascl1/Dlx2* induction, *Ascl1*+Forskolin induction and *NGN2* glutamatergic induction. **M** Example ePSC traces with either fast or slow decay, as measured in the inductions tested here. **N** Histogram of log-transformed decay time constants (decay τ) measured in neurons induced with the four different induction strategies, together with a 'sum of two gaussians' fit (grey line). **O** Pie-charts showing the percentages of neurons with a slow ($\tau \geqslant 30$ ms), intermediate ($6 > \tau < 30$ ms) and fast ($\tau \leqslant 6$ ms) decay, as well as the percentage of synaptically silent neurons, of neurons generated with the four different induction strategies.

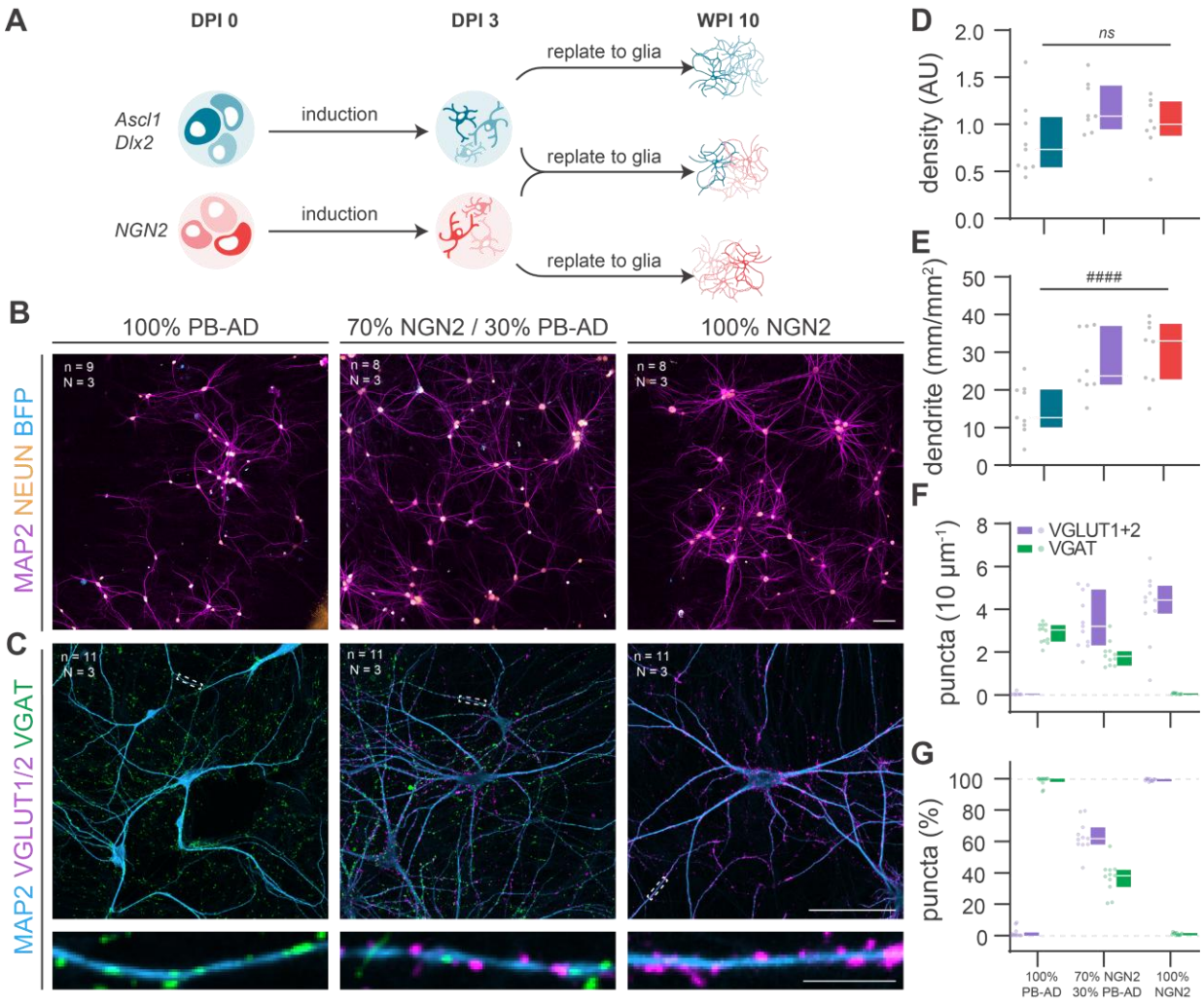

Figure 2. PiggyBac Ascl1/Dlx2 neurons integrate into well-defined excitatory/inhibitory networks upon co-culturing with NGN2 induced neurons

A Schematic of co-culturing protocol in which PiggyBac (PB) Ascl1/Dlx2 (AD) neurons were co-cultured with glutamatergic NGN2 induced neurons to generate excitatory/inhibitory (E/I) co-cultures **B** Representative images of E/I co-cultures at different ratios in which dendrites and neuronal nuclei are visualised using MAP2 and NeuN staining, respectively, and PB-AD neurons visualised by nuclear mTagBFP signals. The E/I-ratio is indicated above each image. Scale bar = 100 µm. **C** Representative images of E/I co-cultures at the same ratios as depicted in (B), stained for MAP2 as dendritic marker and VGAT and VGLUT as markers for GABAergic and glutamatergic synapses, respectively. Scae bars = 100 µm, scale bar zoom in = 10 µm **D** The network density (number of nuclei/field of view) is stable across E/I co-culture ratios. **E** The total dendrite length per field of view decreases as the percentage of plated PB-AD neurons increases. **F** The density of glutamatergic (VGLUT⁺ puncta) and GABAergic (VGAT⁺)

1504 puncta scales with the percentage of NGN2 and PB-AD neurons plated. **G** Synapse counts
1505 shown in F expressed as the percentage of all synapses counted.
1506

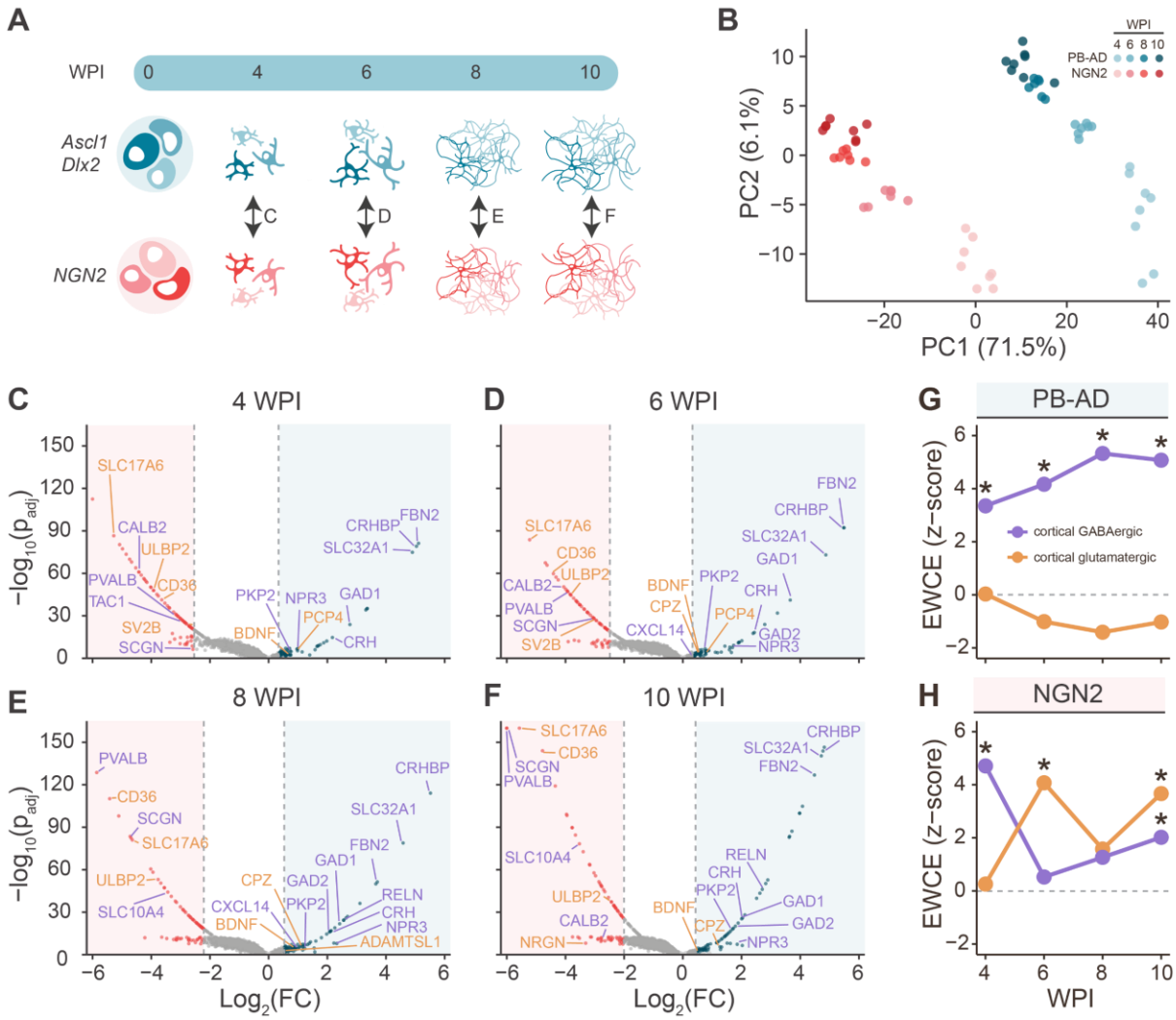

Figure 3. PiggyBac Ascl1/Dlx2 neurons have a cortical GABAergic proteomic profile.

A. Schematic overview of the proteomics analysis in which PiggyBac (PB) Ascl1/Dlx2 (AD) rat astrocyte co-cultures were compared to NGN2 co-cultures per timepoint. Double-sided arrows indicate the contrasts used for analysis. **B**. PCA analysis on neuronal protein abundances reveals separation of culture types as well as time points along the first two components (PC1: 61.7% and PC2: 8.0%). **C-F**. Volcano plots showing regulation of neuronal proteins in PB-AD cultures and in NGN2 cultures at 4 WPI (**C**), 6 WPI (**D**), 8 WPI (**E**) and 10 WPI (**F**). The top 5% significantly upregulated neuronal proteins in PB-AD are shown as blue dots and those in NGN2 as red dots. Proteins are considered significantly regulated if their adjusted p-value is < 0.05 (significance threshold overlaps with x-axis at this scale and is not shown for clarity of the figure) and their $\log_2$ (FC) lies above the 95th or below the 5th percentile (vertical dashed lines). Label colours indicate the predicted cell types based on

1521 cell type specificity scores (CTSS): regulated GABAergic (purple) and glutamatergic proteins
1522 (orange). Cell type specificity was defined using the following CTSS cutoffs: neuronal proteins
1523 (neuronal CTSS>70%), GABAergic proteins (GABAergic CTSS > 80% and glutamatergic CTSS
1524 < 10%), glutamatergic proteins (glutamatergic CTSS > 80% and GABAergic CTSS < 10%). CTSS
1525 can be found in Figure S6. **G**. EWCE analysis of top 5% upregulated neuronal proteins in PB-
1526 AD cultures reveals specific enrichment for GABAergic neurons, which increased up to 8 WPI.
1527 **H**. EWCE analysis of the top 5% upregulated neuronal proteins in NGN2 cultures reveals
1528 significant enrichment for both glutamatergic and GABAergic neurons depending on the
1529 timepoint.
1530
1531
1532

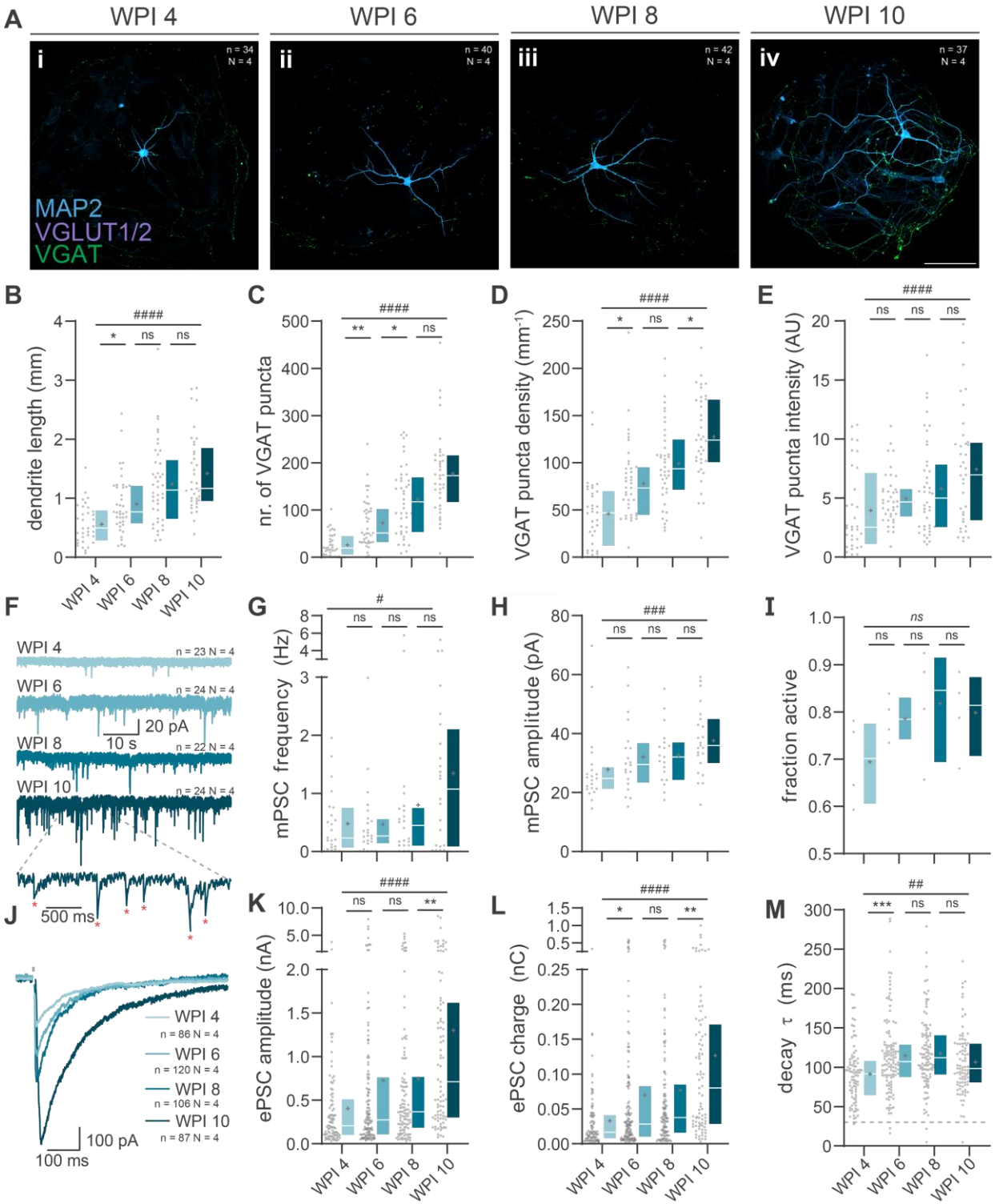

Figure 4. Morphological and functional development of PiggyBac Ascl1/Dlx2 induced neurons

A Typical examples of PB-AD autaptic neurons at WPI 4 (i), 6 (ii), 8 (iii) and 10 (iv). Scale bar: 100 µm **B** Total dendrite length quantified. **C** number of GABAergic synapses per neuron. **D**

1538 Synaptic density. **E** Average VGAT puncta intensity in arbitrary units (AU). Scale bars: 100 µm.
1539 Boxplot whiskers extend the entire data range. **F** Representative traces of mPSCs recorded
1540 from PiggyBac (PB) *Ascl1/Dlx2* (*AD*) neurons (PB-AD) neurons at 4, 6, 8 and 10 weeks post
1541 induction (WPI). **G** mPSC frequency and **(H**) amplitude of PB-AD neurons at 4, 6, 8 and 10
1542 WPI. **I** Boxplots of the average fractions of synaptically active cells at 4, 6, 8 and 10 WPI.
1543 Markers represent averages of individual inductions. **J** Representative ePSC traces of at 4, 6,
1544 8 and 10 WPI. **K** Amplitude, charge (**L)** and decay time (**M**) constant of ePSCs recorded from
1545 PB-AD neurons at 4, 6, 8 and 10 WPI.

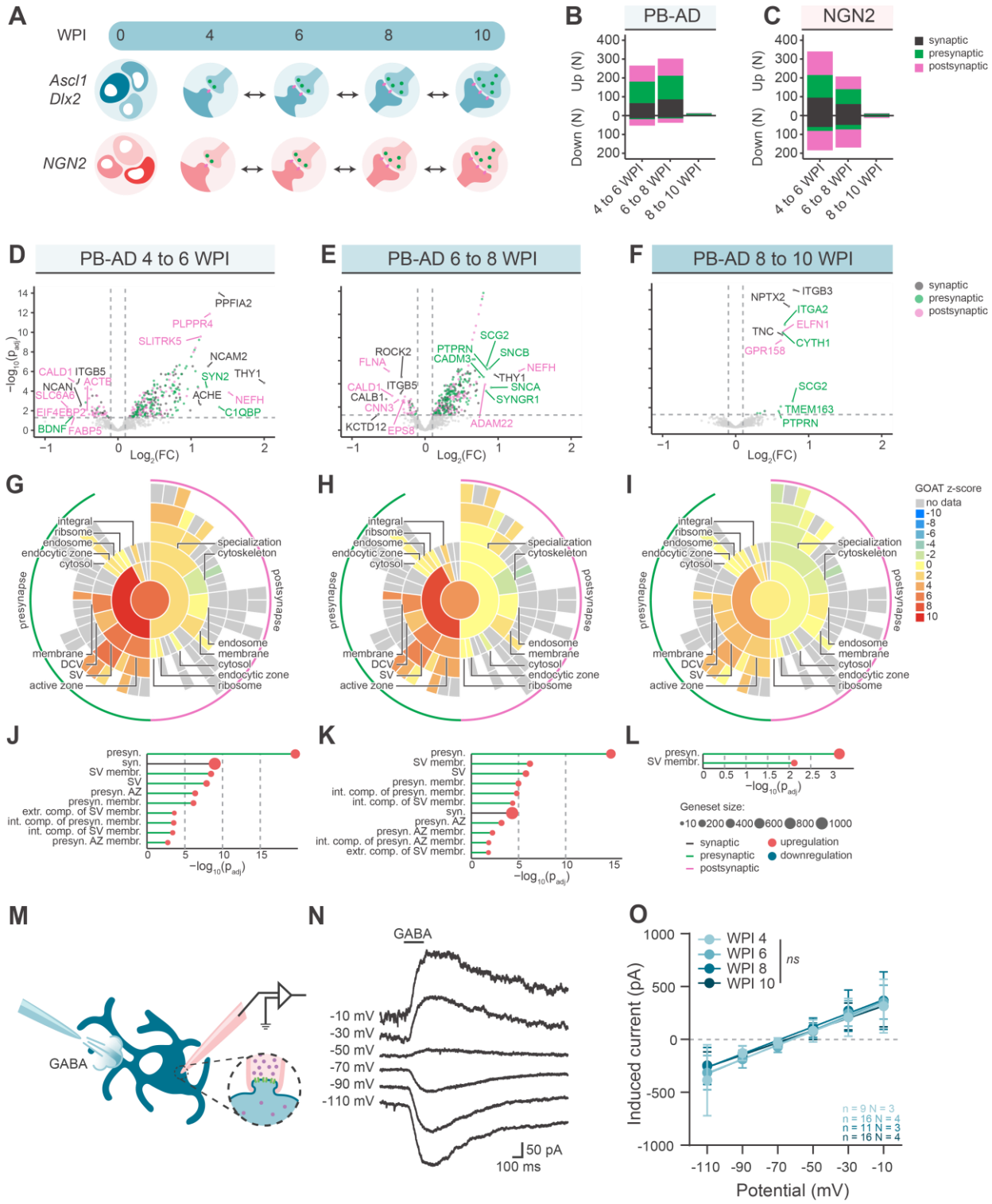

Figure 5. Pre- and postsynaptic maturation of PiggyBac Ascl1/Dlx2 neurons

A. Schematic overview of the proteomics analysis with double-sided arrows indicating the contrasts used for analysis. **B-C**. Stacked bar plots showing the number of up- and

downregulated SYNGO annotated proteins over time, distinguishing synaptic (black), exclusively presynaptic (green) and exclusively postsynaptic (magenta) proteins for PB-AD (**B**) and NGN2 (**C**) neurons. Classifications were assigned based on SynGO annotations, synaptic classification contains both pansynaptic and ambiguously localized synaptic proteins. Regulated proteins have a $\log_2$ (FC) > 0.1, or < -0.1, and adjusted p-value < 0.05. **D-F.** Volcano plots showing regulation of synaptic proteins between 6 and 4 (**D**), 8 and 6 (**E**), and 10 and 8 WPI (**F**). Only SYNGO-annotated proteins are plotted and colour coding refer to significantly regulated synaptic (black) exclusively presynaptic (green) or postsynaptic (pink) annotations. Proteins were regarded significantly regulated when adjusted p-value < 0.05 (dashed horizontal line) and $\log_2$ (FC) > 0.1 or < -0.1 (dashed vertical lines). Top 5% proteins regulated proteins were labelled based on 97.5th and 2.5th percentiles marking genes that drive subsequently detected enrichments. **G-I**. SYNGO plots showing enrichment scores (z-scores) derived from gene-set enrichment analysis with GOAT on SYNGO cellular compartment gene sets, using differential expression output of 6 vs 4 (G), 8 vs 6 (H) and 10 vs 8 WPI (I),. Negative z-scores reflect enrichments primarily driven by downregulated proteins and vice versa for positive z-scores. **J-L.** Lollipop charts showing significant ontologies with their corresponding adjusted p-values and the number of genes part of the gene set as analysed by GOAT for 6 vs 4 (J), 8 vs 6 (K) and 8 vs 10 WPI (L) **M.** Schematic overview of the GABA puff experiment, in which perforated-patch was performed on PB-AD neurons in E/I-networks and GABA was applied to measure the postsynaptic current it produced. **N.** Typical example of the postsynaptic current produced by GABA puff at different holding voltages. **O.** Linear fit of PSC amplitudes as measured in response to GABA puff at 4, 6, 8 and 10 WPI. Error bars represent the SD.

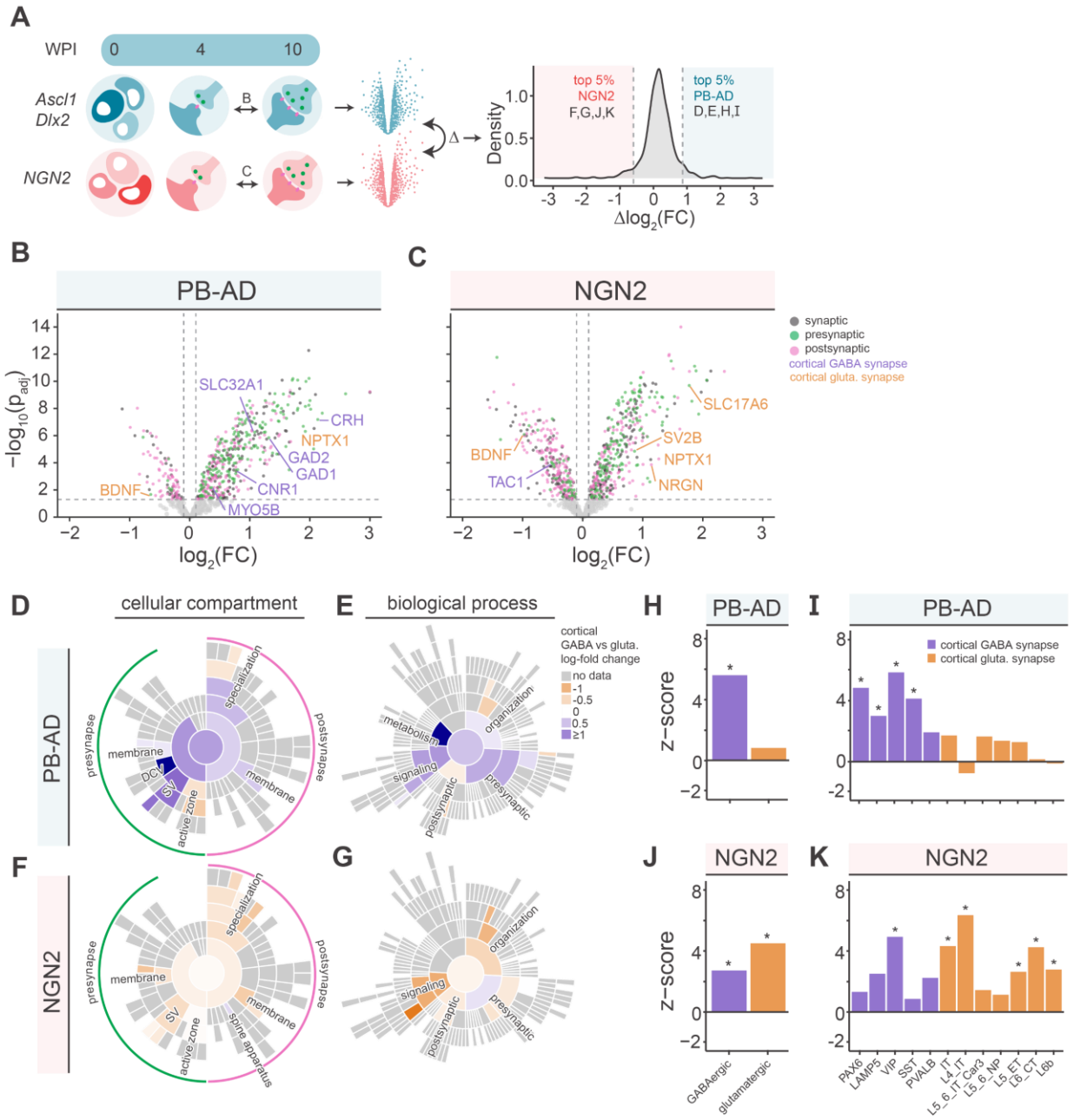

Figure 6. Specialization of PiggyBac Ascl1/Dlx2 and NGN2 neurons into cortical subtypes

A. Schematic overview of the proteomics analysis pipeline. The differential expression of synaptic proteins over time (10 vs 4 WPI) was first quantified for PB-AD and NGN2 culture separately. The difference in expression over time between PB-AD and NGN2 (delta- $\log_2$ (FC)) was next calculated, enabling identification of proteins with PB-AD- or NGN2-specific temporal profiles. Density plot showing 5th and 95th percentiles (dashed vertical lines) selections of proteins that have strong differential temporal regulation (i.e., high or low

1585 delta- log_2 (FC)) in PB-AD compared to NGN2, and vice versa. **B-C**. Volcano plots showing
1586 regulation of synaptic proteins between 10 and 4 WPI. Proteins are considered regulated
1587 when the log_2 (FC) > 0.1 or < -0.1 (dashed vertical lines) and adjusted p-value < 0.05 (dashed
1588 horizontal line). Only SYNGO-annotated proteins are plotted, and dot colors refer to
1589 significantly regulated synaptic (black) exclusively presynaptic (green) or postsynaptic (pink)
1590 annotations. Label colours indicate for predicted cortical GABAergic- (purple) or
1591 glutamatergic (orange) regulated proteins. **D-G** SYNGO sunburst plots showing the
1592 GABAergic and glutamatergic specification of PB-AD and NGN cultures. The SYNGO sunburst
1593 inputs are the proteins that are part of the 5th (**F-G**) and 95th percentiles (**D-E**) from the delta-
1594 log_2 (FC) distribution (**A**), which represent the top 5% exclusively PB-AD and NGN2 regulated
1595 proteins, respectively. GABAergic or glutamatergic annotation for these SYNGO terms is
1596 estimated based on the differential RNA expression (log_2 (FC)) between cortical GABAergic
1597 and glutamatergic neurons of corresponding genes[40] Both cellular compartment (**D-F**) and
1598 biological process (**E-G**) gene sets were used. **H-K**. EWCE analysis of PB-AD-specific (**H-I**) or
1599 NGN2-specific proteins (**J-K**) show enrichment for GABAergic and glutamatergic cell sub
1600 (classes), respectively. IT and ET refer to intra- and extratelenchephalic-projecting neurons
1601 and NP refers to near-projecting neurons.[40]
1602

1603 **Supplementary figures and table**

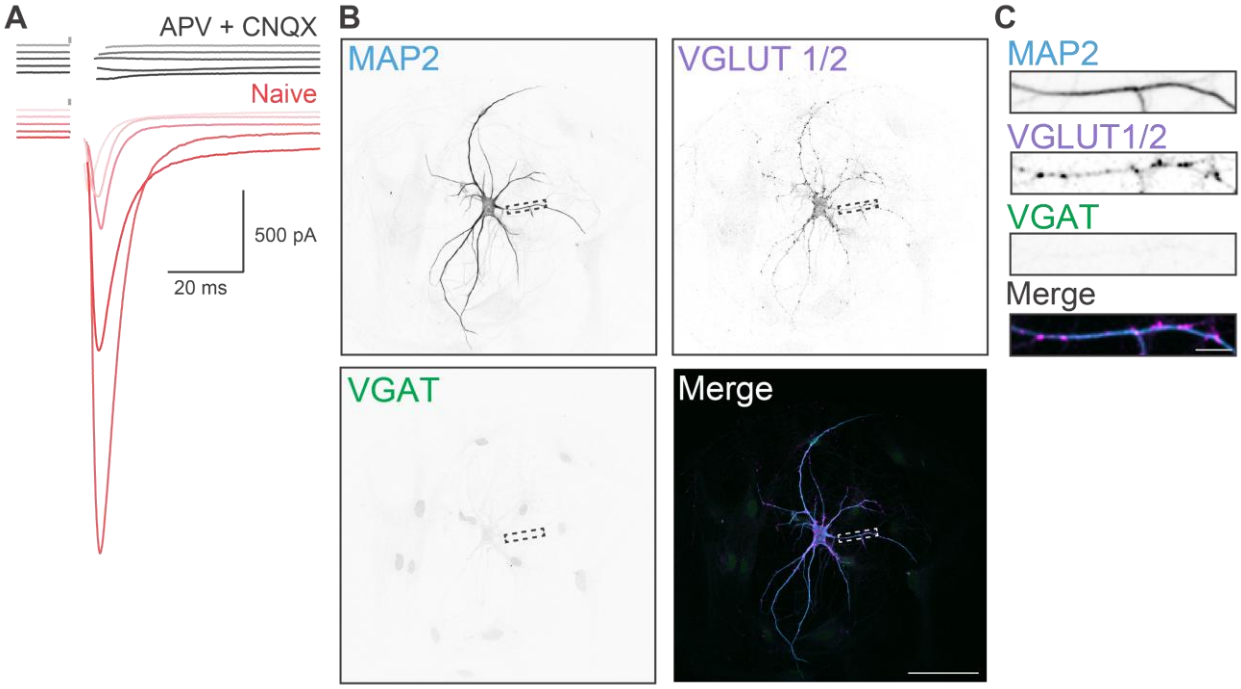

1604

1605 *Figure S1. NGN2 neurons produce glutamatergic transmission*

1606 **A** Voltage clamp recordings of 6 WPI NGN2 autaptic neurons after stimulation, in normal
1607 ACSF (Naive) and in presence of glutamatergic receptor blockers (APV + CNQX). Synaptic
1608 transmission was fully abolished by blockers, illustrating that NGN2 neurons are
1609 glutamatergic. **B-C** Examples of immunocytochemistry for MAP2, VGAT and VGLUT1+2
1610 performed on NGN2 autaptic neurons, with zoom in on a length of dendrite (**C**). Scale bar =
1611 100 µm, zoom in scale bar = 10 µm

1612

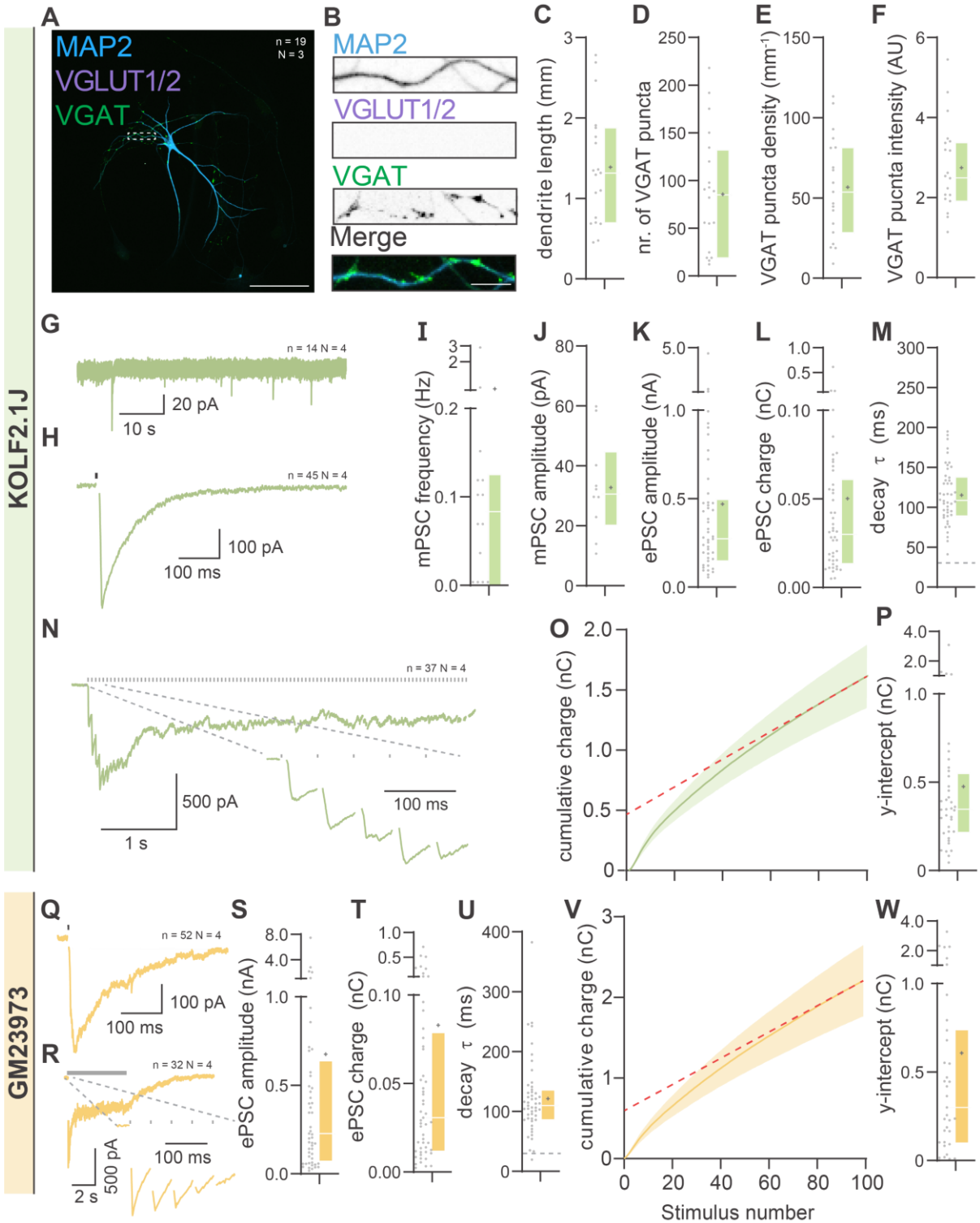

Figure S2. PiggyBac Ascl1/Dlx2 induction reliably generates GABAergic neurons in the KOLF2.1J and GM23973 line

A Representative images of PiggyBac (PB) Ascl1/Dlx2 (AD) neurons induced from KOLF1.2J iPSCs at 7 weeks post induction (WPI), stained for MAP2 as dendritic marker, and VGAT and VGLUT1/2 as GABAergic and glutamatergic markers, respectively. Scale bar: 100 µm **B** Zoom-

in on dendrite to illustrate punctate VGAT staining. Scale bar: 10 μm **C.** Total dendrite length and (**D**) number of GABAergic synapses per neuron. **E** Synaptic density and intensity (**F**). **G** Representative mPSC trace and (**H**) representative ePSC trace from PB-AD neurons induced from the KOLF2.1J line. **I** Frequency and (**J**) amplitude of miPSCs. **K** Amplitude, (**L**) charge and (**M**) decay time constant of iPSCs in PB-AD neurons generated from the KOLF2.1J line. **N** Representative trace of iPSCs evoked by 20Hz stimulation trains with zoom-in on first five pulses in KOLF2.1J. **O** Plot of cumulative iPSC amplitudes evoked by 20 Hz stimulus trains, with back-extrapolated linear fits displayed in red. **P** RRP estimate obtained from back-extrapolation of linear fits displayed in (**M**). **Q**. representative ePSC traces from PB-AD neurons induced from the GM23973 line. **R.** Representative trace of iPSCs evoked by 20Hz stimulation trains with zoom-in on first five pulses in GM23973. **S** Amplitude, (**T**) charge and (**U**) decay time constant of iPSCs in PB-AD neurons generated from the GM23973.1J line. **V** Plot of cumulative iPSC amplitudes evoked by 20 Hz stimulus trains, with back-extrapolated linear fits displayed in red. **W** RRP estimate obtained from back-extrapolation of linear fits displayed in (M). Boxplot whiskers extend the entire data range.

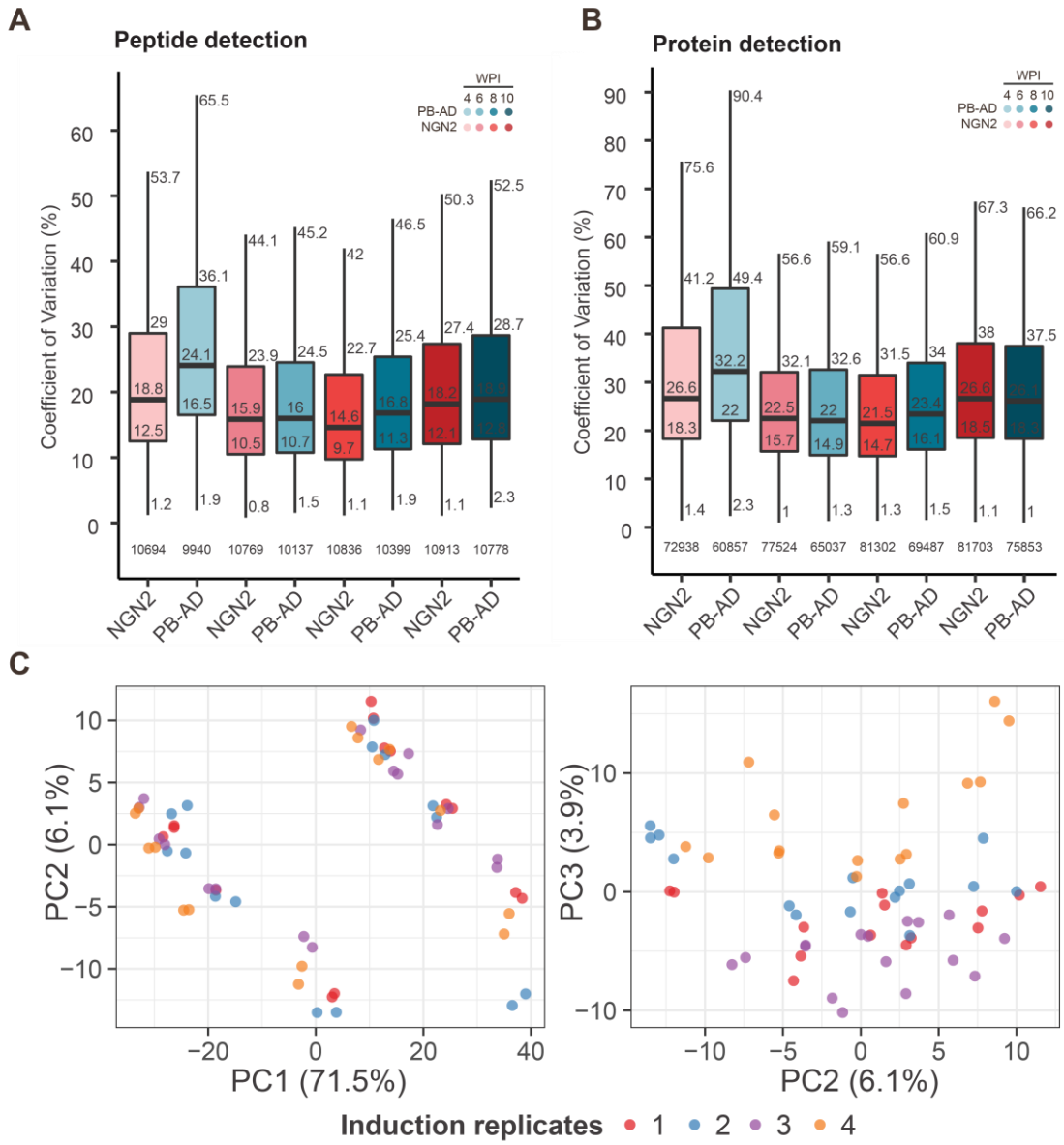

Figure S3. Peptide and protein detection count and variation is similar between cultures and timepoints.

A-B Boxplots showing variation of peptide (**A**) and protein (**B**) detection for all timepoints per culture, indicating median, 1st and 3rd quartiles, and minimum and maximum values. Number of detected peptides and proteins are indicated in the base of the graph. Median coefficient of variation for peptide and protein detection across groups ranged from 14.6% to 32.2%, reflecting consistent detection performance across replicates. **C** PCA plots showing potential batch effects due to induction. PC1 and PC2 show even spread of different inductions but PC3 (3.9%) shows slight separation based on induction and we therefore corrected for induction effect when performing differential abundance analysis.

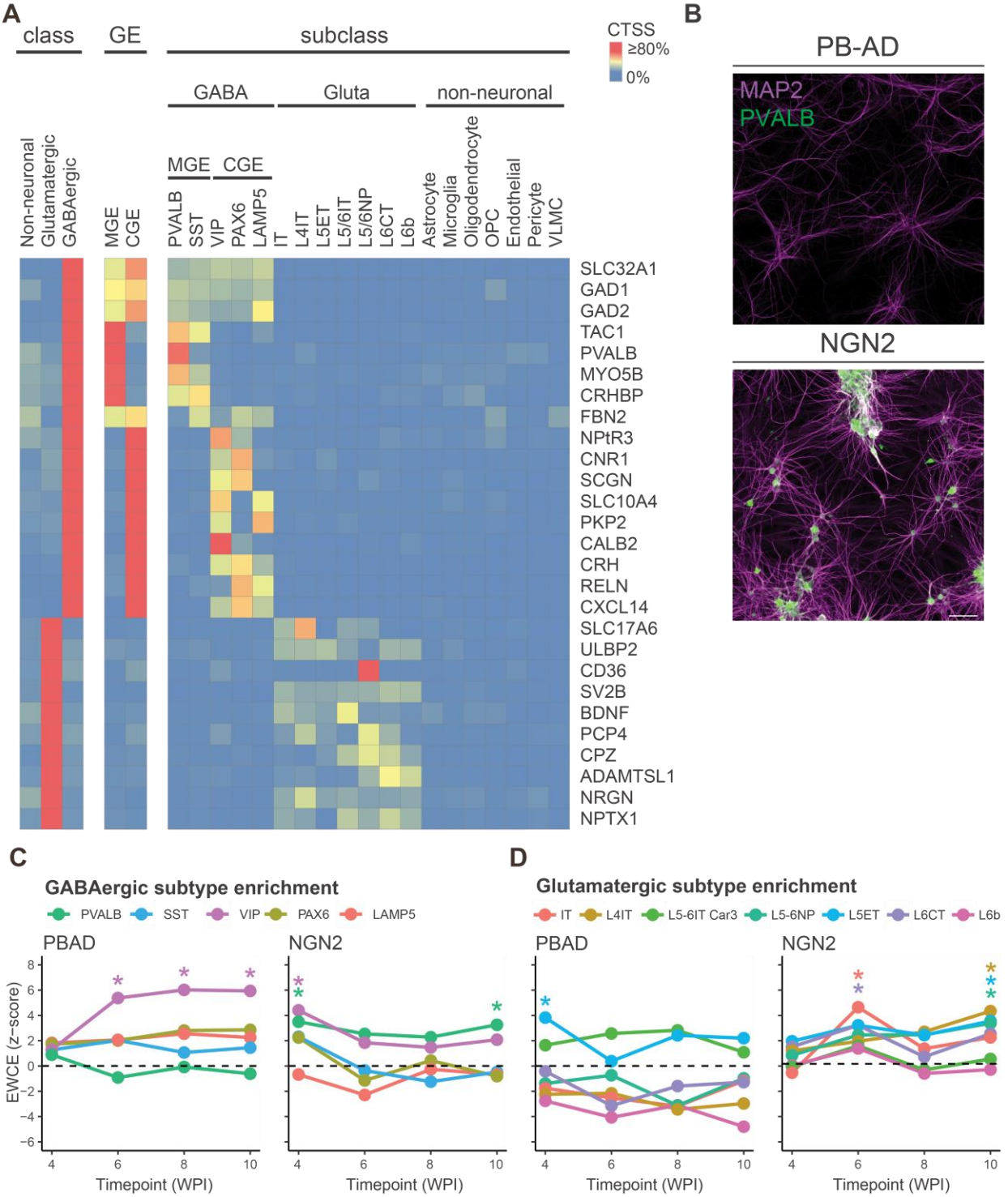

Figure S4. Cell type specificity scores for detected GABAergic proteins

A. Cell type specificity scores (CTSS) scores for detected GABAergic and glutamatergic proteins. CTSS are calculated with the expression weighted cell type enrichment tool.[41]

using single-cell RNA-sequencing data from Jorstad et al. [40] MGE and CGE refer to medial and caudal ganglionic eminences. **B.** Representative images of PB-AD and NGN2 neurons stained for MAP2 and PVALB. Scale bar = 100 µm. **C-D** Expression-weighted cell type enrichment (EWCE) analysis showing enrichment of proteins higher expressed in PB-AD or NGN2 for GABAergic **(C)** and glutamatergic subtypes **(D)**. PBAD-enriched proteins showed strongest enrichment for VIP^+ interneurons at most timepoints, whereas NGN2-enriched proteins map at different timepoints to both GABAergic ($PVALB^+$ and VIP^+ interneurons) and glutamatergic subtypes. PB-AD-enriched proteins showed unexpected enrichment for L5ET neurons at 4 WPI, which reduced below significance threshold at later timepoints. IT and ET refer to intra- and extratelenchephalic-projecting neurons, and NP refers to near-projecting neurons – cell subclass annotations consistent with Jorstad et al. (2023).[40]

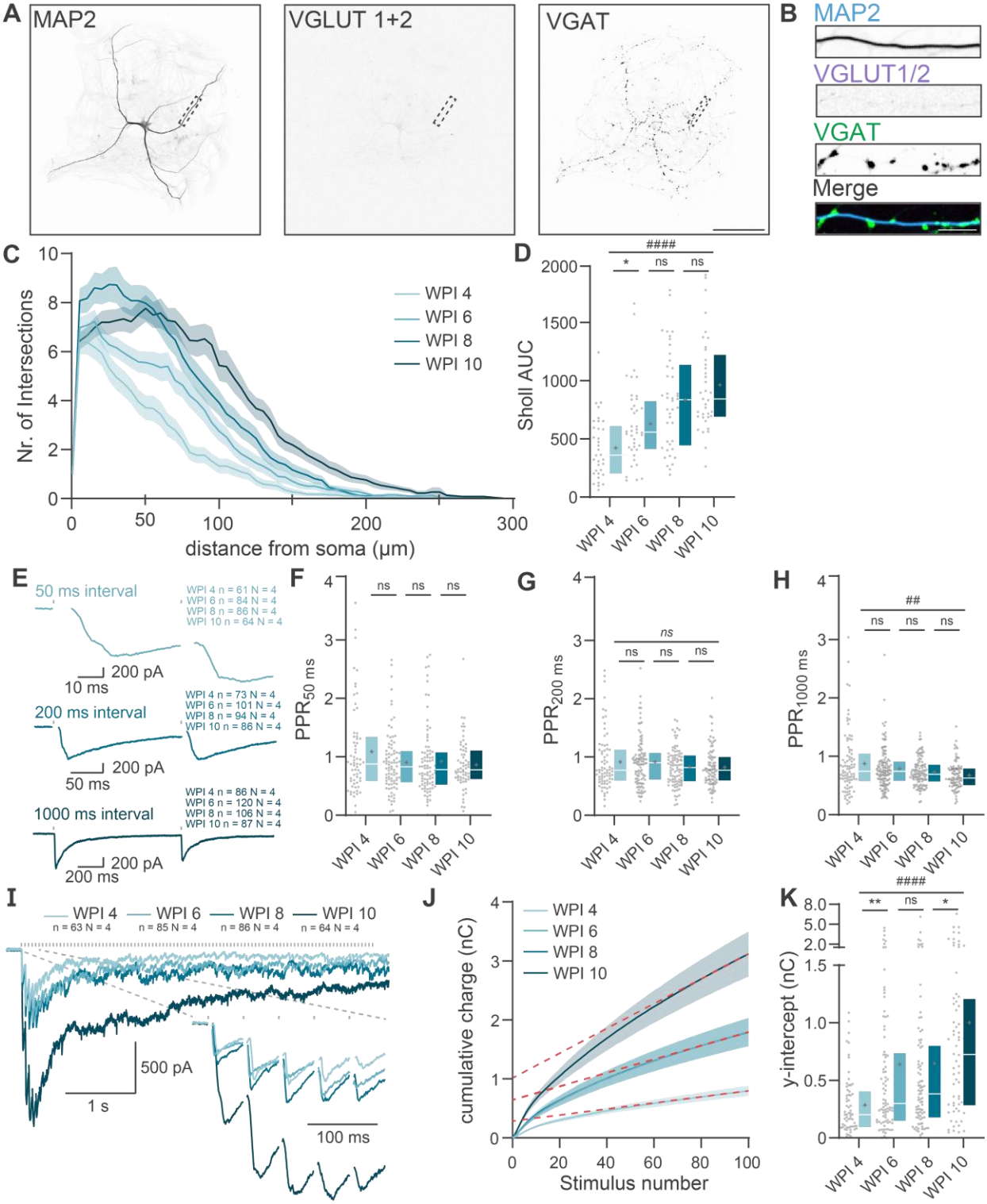

Figure S5. Extended morphological and functional development of PiggyBac Ascl1/Dlx2 induced neurons

A Representative images of an autaptic PiggyBac (PB) *Ascl1/Dlx2* (AD) induced neuron at week-post-induction 10, stained for MAP2 as dendritic marker, and VGAT and VGLUT1/2 as GABAergic and glutamatergic markers, respectively. Scale bar: 100 µm **B** Cut-out of dendrite

1665 marked in A to illustrate individual synaptic puncta. Scale bar: 10 µm **C** Sholl analysis of PB-
1666 AD autaptic neurons at WPI 4, 6, 8 and 10. Shaded areas represent the SEM. **D** Quantification
1667 of the area under the curve (AUC) of the Sholl histogram shown in (**C**) **E** Representative traces
1668 of paired-pulse ePSCs at a 50, 200 and 1000 ms interval at 10 WPI. **F** Quantified paired-pulse
1669 amplitude ratios (PPR) at a 50 ms, 200 ms (**G**) and 100 ms (**H**) interval at 4, 6, 8 and 10 WPI. **I**
1670 Representative traces of iPSCs evoked by 20Hz stimulus trains from PB-AD neurons at 4, 6,
1671 8 and 10 WPI with zoom in on first five pulses. **J** Plot of cumulative iPSC charge evoked by
1672 20 Hz stimulus trains, with back-extrapolated linear fits displayed in red. Note, WPI 4 and
1673 WPI 6 data overlap. **K** RRP estimate obtained from back-extrapolation of linear fits displayed
1674 in (**J**).

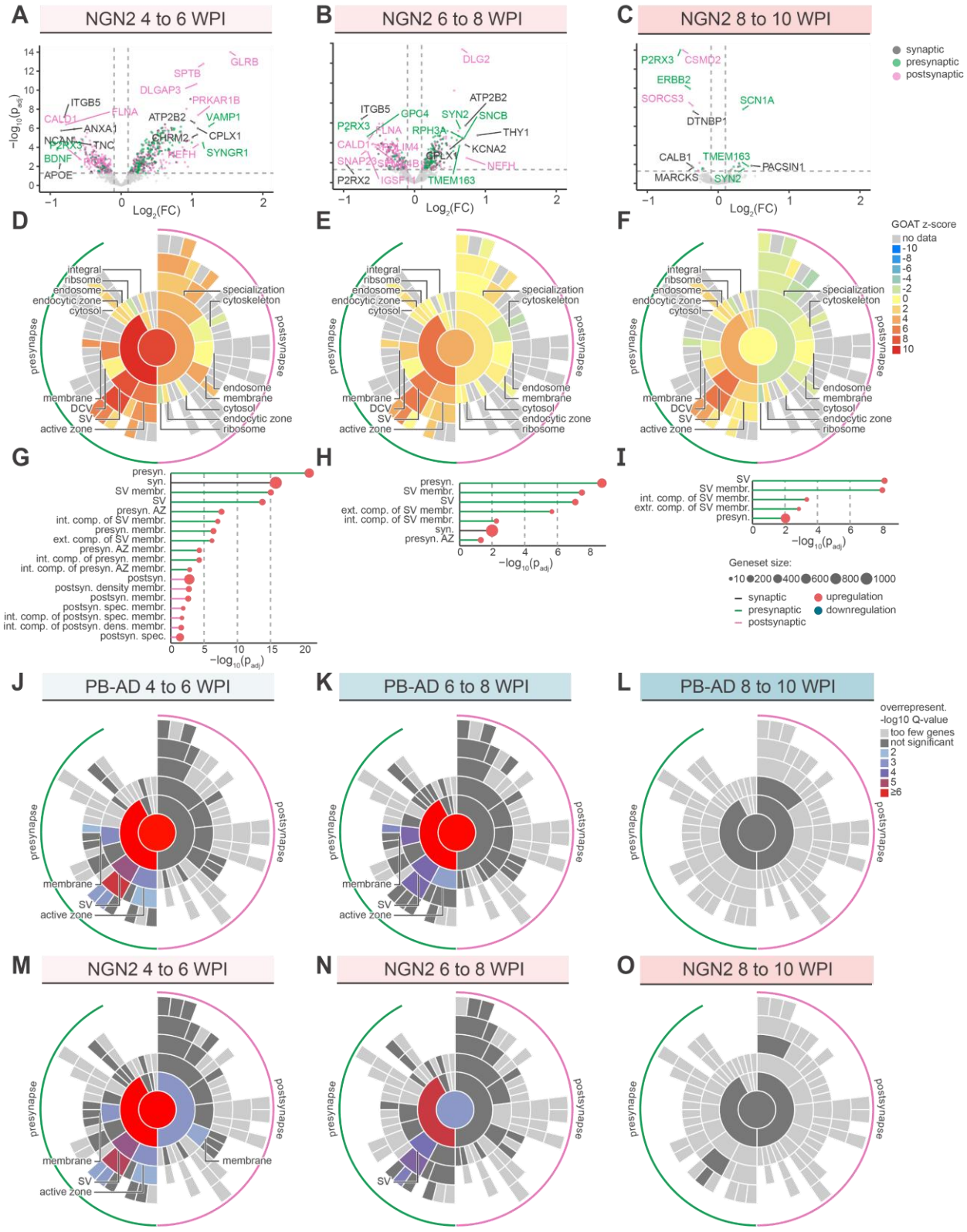
A
NGN2 4 to 6 WPI
B
NGN2 6 to 8 WPI
C
NGN2 8 to 10 WPI
synaptic
presynaptic
postsynaptic
Log2(FC)
D
E
F
GOAT z-score
no data
presynapse
postsynapse
integral
ribsome
endosome
endocytic zone
cytosol
specialization
cytoskeleton
membrane
DCV
SV
active zone
ribosome
G
H
I
Geneset size:
synaptic
presynaptic
postsynaptic
upregulation
downregulation
J
PB-AD 4 to 6 WPI
K
PB-AD 6 to 8 WPI
L
PB-AD 8 to 10 WPI
overrepresent.
-log10 Q-value
too few genes
not significant
M
NGN2 4 to 6 WPI
N
NGN2 6 to 8 WPI
O
NGN2 8 to 10 WPI

1675

1676 *Figure S**6**. Differential expression of synaptic genes in NGN2 and PB-AD neurons*
1677 **A-C.** Volcano plots showing regulation of synaptic proteins in NGN2 cultures between 6 and
1678 4 (**A**), 8 and 6 (**B**), and 10 and 8 WPI (**C**). Only SYNGO-annotated proteins are plotted and
1679 colour coding refer to significantly regulated synaptic (black) exclusively presynaptic (green)
1680 or postsynaptic (pink) annotations. Proteins were regarded significantly regulated when
1681 adjusted p-value < 0.05 (dashed horizontal line) and $\log_2$ (FC) > 0.1 or < -0.1 (dashed vertical
1682 lines). **D-F**. SYNGO plots showing enrichment scores (z-scores) derived from gene-set
1683 enrichment analysis with GOAT using SYNGO cellular compartment gene sets for 4 to 6 (**D**),
1684 6 to 8 (**E**) and 8 to 10 WPI (**F**). Negative z-scores (blue) reflect enrichments primarily driven
1685 by downregulated proteins and vice versa for positive z-scores (red). **G-I.** Lollipop charts
1686 showing significant SYNGO terms with their corresponding adjusted p-values and the
1687 number of genes part of the gene set. **J-O.** SYNGO overrepresentation analysis of upregulated
1688 proteins in PB-AD (**J-L**) and NGN2 (**M-O**) per timepoint. Foreground are significantly
1689 upregulated proteins and background are all tested genes in corresponding contrast.

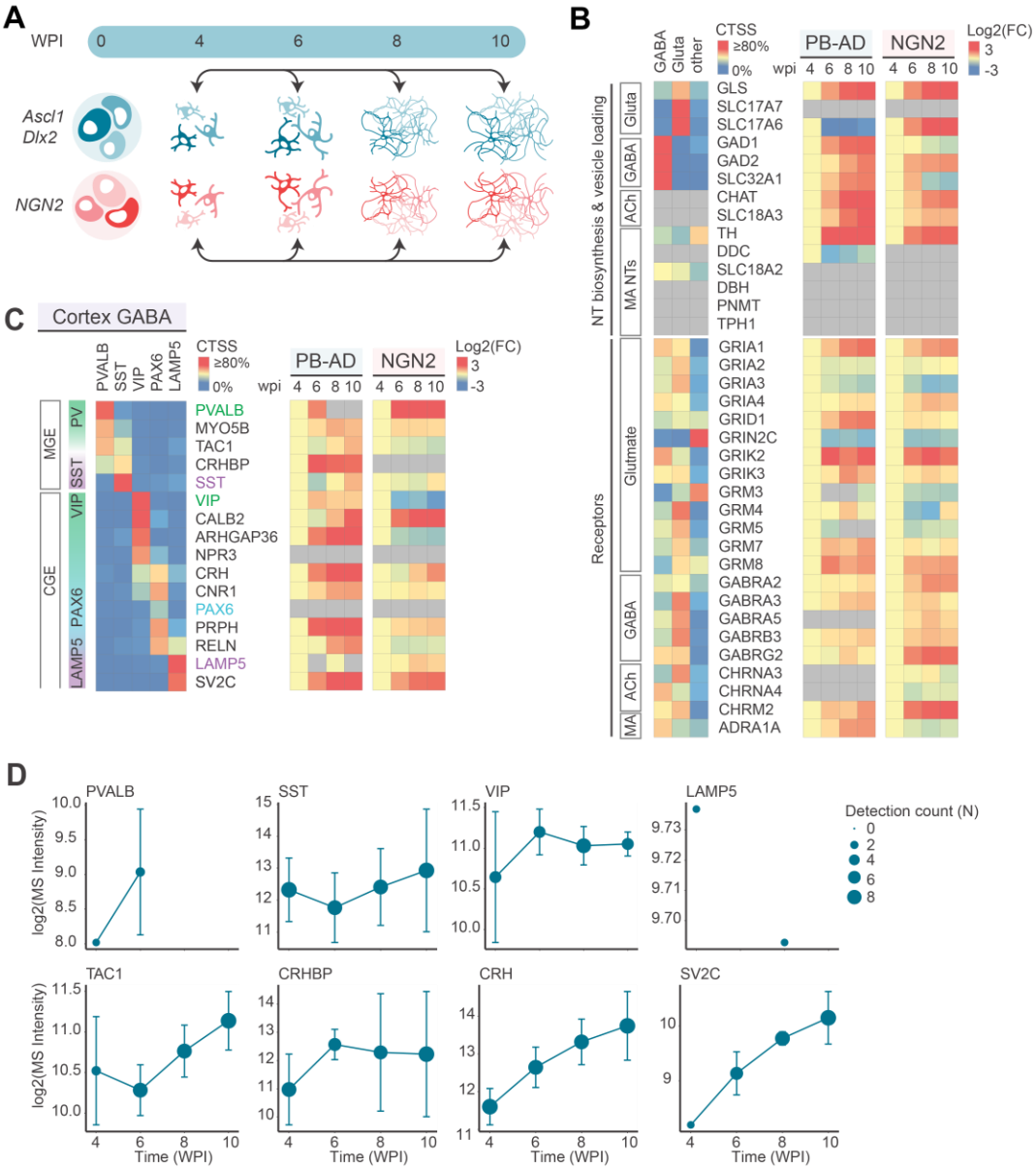

Figure S7. PiggyBac Ascl1/Dlx2 and NGN2 neurons express markers of diverse GABAergic neuron subtypes

A. Contrasts used to determine cell type specification. **B** and **C** Heatmaps that show temporal expression profiles relative to 4 WPI ($\log_2$ (FC)) and cell type specificity scores (CTSS). **B** Typical proteins required for neurotransmitter (NT) synthesis, vesicle loading, and receptors. Undetected proteins are visualized for NT biosynthesis and vesicle loading but not for receptors. **C** Canonical GABAergic subtype markers and proteins with high cell type specificity for GABAergic subtypes and for medial or caudal ganglionic eminences (MGE or CGE). **D.** Line plots show sum expression of canonical GABAergic subtype markers (top) and other proteins with GABAergic cell type specificity. Error bars represent SD and dot size indicate detection count.

1701 *Supplemental table 1: SYNGO Proteins with significant expression changes from 8 to 10 WPI in PB-AD neurons*

Protein	**new at WPI 10**	**log_2fc**	**FDR-adjusted p-value**
CNTNAP4	yes	1.05	1.50E-26
SLITRK1	yes	0.97	7.75E-23
CDH1	yes	0.91	4.81E-20
EPHA7	yes	0.90	1.26E-19
ITGB3	no	0.80	1.72E-15
PRRT1	yes	0.74	1.35E-13
NPTX2	no	0.73	4.68E-13
ITGA2	no	0.67	3.46E-11
SLC17A5	yes	0.67	5.09E-11
KCNQ2	yes	0.65	1.77E-10
ELFN1	no	0.65	2.09E-10
CYTH1	no	0.65	2.21E-10
TNC	no	0.64	3.74E-10
NRGN	yes	0.63	6.71E-10
NGDN	yes	0.63	6.73E-10
GPR158	no	0.62	1.43E-09
RELN	yes	0.57	3.53E-08
SCG2	no	0.78	2.18E-03
TMEM163	no	0.62	7.64E-03
PTPRN	no	0.59	2.24E-02
NEFH	no	0.40	2.24E-02
IGSF8	no	0.40	2.24E-02
CNTNAP1	no	0.34	3.78E-02
ATP2B4	no	0.30	3.78E-02

1702

1703